Climate adaptation in *P. trichocarpa*: key adaptive loci identified for stomata and leaf traits

Marie C Klein[1], Zi Meng[1], Jack Bailey-Bale[1], Suzanne Milner[1], Peicai Shi[1], Wellington Muchero[2], Jin-Gui Chen[2], Timothy J Tschaplinski[2], Daniel Jacobson[2], John Lagergren[2], Matthew Lane[3], Chris O'Brien[3], Hari Chhetri[2], Chanaka Roshan Abeyratne[2], Mengjun Shu[2], Peter Freer-Smith[1], Thomas N Buckley[1], Troy S Magney[1], J Grey Monroe[1], Gerald A Tuskan[2], Gail Taylor*[1]

[1]Department of Plant Sciences, University of California Davis, Davis, CA 95616, USA.
[2]Biosciences Division and the Center for Bioenergy Innovation, Oak Ridge National Laboratory, Oak Ridge, TN 37831, USA.
[3]Bredesen Center for Interdisciplinary Research and Graduate Education, University of Tennessee Knoxville, Knoxville, TN 37996, USA.

*Correspondence to: gtaylor@ucdavis.edu & current address Department of Genetics, Evolution and Environment, UCL, London, WC1E 6BT, UK

ORCIDs: GT 0000-0001-8470-6390, JGM 0000-0002-4025-5572, TM 0000-0002-9033-0024, TNB 0000-0001-7610-7136, JT 0000-0003-0106-1289, JGC 0000-0002-1752-4201

Abstract

Identifying adaptive genetic variation is a key goal for plant breeding and predicting species responses to climate change. Here, we measured 14 leaf and stomatal traits under control (well-watered) and drought conditions, subsampling a diversity collection of over 1,300 *Populus trichocarpa* genotypes, a potential biofuel feedstock crop. Stomatal traits were correlated with genotypes' climate of origin, with those originating from more arid environments tending to have smaller stomata but with higher density. Genome-Wide Association Studies (GWAS) identified loci underlying this trait diversity. Most notably, we discovered a major-effect locus associated with stomatal size and abaxial contact angle (a proxy for cuticular wax) on chromosome 10 localizing to a tandem array of β-ketoacyl-CoA synthases (KCS) genes. The functional relevance and adaptive value of this locus was further supported by analyses of RNAseq and climate-allele associations. We found evidence that future climates may select for the KCS allele linked to smaller stomata, with the strength of selection depending on changes in aridity. These findings reveal adaptive variation in stomatal and physiological traits along with underlying genetic loci, with implications for evolution and breeding - providing insights into the responses to future climate change.

Keywords

***Populus trichocarpa*, stomata, leaf, drought, bioenergy, climate adaptation**

Highlight

Research on *Populus trichocarpa* reveals adaptation of physiological and stomatal traits linked to drought tolerance, with genotypes from arid regions exhibiting smaller stomata and identifies a key genetic locus for stomatal size, of significance climate change adaptation and sustainable biofuel production.

Abbreviations

CID: Carbon Isotope Discrimination
CO_2: Carbon dioxide
SLA: Specific leaf area (Leaf surface area [mm^2]/ dry mass [mg])
$\delta^{13}C$: ratio of the two stable isotopes of carbon ^{13}C and ^{12}C, a proxy for water use efficiency
GWAS: Genome-wide association study
NDVI: Normalized difference vegetation index
PRI: Photochemical Reflectance Index
RGR: Relative Growth Rate
PWC: Proportional Water Content
SAF: sustainable aviation fuel
WUE: Water-use efficiency

Introduction

Altered rainfall patterns and rising temperatures are intensifying drought depth and occurrence, jeopardizing agricultural output (Cook et al., 2018; Dai, 2012; Food and Agriculture Organization of the United Nations et al., 2018). Moreover, in anticipation of the emerging circular bioeconomy, there is a growing need for fast-growing non-food trees and grasses (Clifton-Brown et al., 2019; Somerville et al., 2010) that can both grow on marginal lands (Hoegh-Guldberg et al., 2018; Mehmood et al., 2017; Schmidt et al., 2015) and tolerate drought and limited nutrient inputs. Consequently, a pivotal challenge is to achieve economically viable yields on marginal lands, in the face of limited water availability (Hoegh-Guldberg et al., 2018; Taylor et al., 2019). Given these challenges, it is crucial to study the physiology and genetics of climate adaptation in potential biofuel crops like poplar (*Populus* spp). Understanding the genetic basis and adaptive value of ecophysiological traits can facilitate the development of varieties that are resilient to arid climates (Blumstein et al., 2020; Savolainen et al., 2013; Stapley et al., 2010).

Collections of diverse genotypes of natural populations in common gardens, originating from wide-ranging environments, are invaluable resources to address these challenges (Taylor et al., 2024). Such collections enable the identification of links between traits and their climates of origin, shedding light on the adaptive value of phenotypic diversity. This can inform predictions of which traits are suitable for dry climates and guide the selection of genotypes for cultivation in arid regions. Additionally, the genetic basis of these traits can be elucidated through this genomic diversity. This exploration is essential for pinpointing genetic markers that can be used to accelerate breeding programs and conservation efforts.

Stomatal traits are central to plant water management and exhibit natural variation in size and density, which have been linked to climate of origin (Beerling & Woodward, 2008; Franks & Beerling, 2009). Smaller and denser stomata, for instance, have often been observed in genotypes from drier

climates, suggesting an evolutionary adaptation to aid water conservation and improve plant water-use efficiency (WUE) (McKown et al., 2019; McKown, Guy, Klápště, et al., 2014; McKown, Guy, Quamme, et al., 2014). This assocation underscores the importance of stomata in local adaptation (Dittberner et al., 2018; Doheny-Adams et al., 2012; Franks et al., 2009; Kardiman & Ræbild, 2018; Ohsumi et al., 2007; Sun et al., 2014). However, the scope of leaf traits influencing water dynamics extends beyond stomata (McKown, Klápště, et al., 2014). Leaf area, leaf mass, specific leaf area (SLA), photosynthetic potential, surface wettability, and integrated rather than instantaneous WUE form an intricate network that characterizes plant interaction with the environment. Each trait contributes to a plant's ability to conserve water, optimize photosynthesis, and survive in varying conditions of water availability (Benavides et al., 2021). Trade-offs between traits that impact water loss and carbon gain are well known, for example, smaller leaves with higher SLA may transpire less water, and larger leaves might capture more light, balancing the trade-offs between water conservation and energy acquisition (Franks & Beerling, 2009; Hetherington & Woodward, 2003; Z. Liu et al., 2020; Wright et al., 2004, 2017; Wu et al., 2016). Similarly, wettability—the degree of water adhesion to the leaf surface, shaped by cuticle properties and microstructure—plays a key role in regulating leaf temperature and transpiration, aiding water conservation in arid environments (Cavallaro et al., 2022). Structural traits, such as trichome coverage and cuticular wax composition, further influence wettability, affecting stomatal function and photosynthetic efficiency (Aparecido et al., 2017), including cuticular wax composition, which serves as a protective barrier against abiotic stresses (Shepherd & Wynne Griffiths, 2006). It can play an adaptive role in drought response through phenotypic plasticity rather than genetic differentiation (Simões et al., 2020).

At the same time, the direct correlation between total plant water use and yield is also well-established, including for poplar, with high-yielding 'water spending' and lower-yielding 'water saving' strategies varying in their usefulness depending on the intensity, longevity, and life-stage of the drought (Tardieu, 2022). Unraveling these conflicting ecological strategies remains challenging.

Although *Populus* trees, as riparian plants, are typically considered vulnerable to drought, notable differences in drought response have been documented among *Populus* genotypes (Cocozza et al., 2010; Huang et al., 2009; Marron et al., 2002; Monclus et al., 2006; Regier et al., 2009; Street et al., 2006; Tschaplinski et al., 1994, 2006; Viger et al., 2013) and the genus can be found across contrasting climate zones, including in extremely arid environments (Brosché et al., 2005). Recognized for its fast growth and high cellulose content, *Populus trichocarpa* stands out as a promising bioenergy crop, including for liquid biofuel production alongside Bioenergy with Carbon Capture and Storage (BECCS). In addition, *Populus* is a valuable model for genetics and plant biology research (Kačík et al., 2012; Taylor et al., 2019; Tuskan et al., 2006) and extensive research has provided substantial evidence of local adaptation to the climatic conditions of its native habitats (McKown et al., 2014; Evans et al., 2014, 2016; Porth et al., 2015; Zhang et al., 2019; Blumstein et al., 2020; Apuli et al., 2021). Such attributes augment the significance of *P. trichocarpa* trees in achieving the U.S. Department of Energy's ambitious Sustainable Aviation Fuel (SAF) target by 2050, while simultaneously reducing life cycle greenhouse gas emissions by at least fifty percent (U.S. Department of Energy, 2022).

To assess the degree of local adaptation of leaf and stomatal traits, we established a common garden of black cottonwood (*Populus trichocarpa*) in Davis, California, an extremely hot and dry site. These trees are derived from a natural population from the Pacific Northwest, representing a wide spectrum of climates (Evans et al., 2014; Gornall & Guy, 2007; McKown, Guy, Klápště, et al., 2014). In this study, we investigated the role and importance of 14 leaf physiology traits related to leaf morphology, stomata, and water use in *P. trichocarpa* under both drought and well-watered conditions. We conducted

field campaigns to measure leaf and stomatal traits twice during the summer growing season in a subsample of approximately 469 unique genotypes (**Figure 1, Supplemental Figure S1d-e Supplemental Table 1**). We measured biomass yield traits in the whole population (approximately 1382 unique genotypes). In doing so, we explore the adaptive signature of drought tolerance and plastic responses in this widely divergent population. To overcome the difficulties associated with phenotyping a large number of samples, we employed a suite of automated phenotyping algorithms for data acquisition. Among leaf traits, we also assessed $\delta^{13}C$ of approximately 469 unique genotypes — a metric for WUE in wood sampled during tree dormancy, shown in *Populus* to be valuable and correlated with WUE (Bogeat-Triboulot et al., 2019; Viger et al., 2016). The goal of our study was to explore the relationship between trait variation and climate of origin, assessing the adaptive value of trait variation, their relevance and usefulness to trait selection for drought tolerance, and the roles of plastic acclimatory responses. Finally, genome-wide association analyses were conducted to characterize the genetic basis of these traits, enabling a more holistic view of climate-genotype-trait relationships in *P. trichocarpa* that reflects local adaptation and provides gene targets for future tree improvement for the emerging bioeconomy.

Materials and Methods

Field Site and Plant Material

The research was conducted on a 6.1-hectare plot at the UC Davis Plant Science Field Facility in Davis, CA (38°32’47.4’’N, 121°47’32.7’’W) **(Figure 1a)** as described previously (Taylor et al., 2024). The experimental layout of the whole site consisted of drought and control treatments across adjacent fields divided into three distinct blocks arranged in an incomplete randomized block design. The *P. trichocarpa* population used in this study was sourced from a range of latitudes exhibiting diverse climate and rainfall patterns representative of most of the species habitats (38.9-54.3°N, 116-128.7°W) and included 1382 genotypes total **(Figure 1a)**. *P. trichocarpa* cuttings were received and planted in a greenhouse on February 1st, 2020. On March 30, 2020, they were relocated to a lath house to harden. Subsequently, 7,628 trees were transplanted to the field on April 10, 2020, with 782 unique genotypes in the drought field site and 1382 unique genotypes in the control field site, reflecting the availability of viable cuttings. A single row of *P. trichocarpa* border trees (not used for measurements) was established around the experimental trees in each replicate block to reduce the effect of undesired edge effects.

Drought Treatment

We employed surface drip irrigation, applying a set water volume measured with flow meter sensors, OMNI™+ Turbo (T^2) Water Meters, at each treatment site throughout the field season. Trees were fully irrigated until March 2021 to conclude their first establishment year. Following this, the irrigation was reduced in the drought treatment to achieve a soil moisture deficit of 150 centibars (0.15 MPa) from March to December 2021. This deficit was significant in comparison with the fully irrigated (control) treatment, representing a long-term modest drought throughout the growing season. During the 2021 field season, soil moisture was monitored using Watermarks (Granular Matrix Sensors from MMM) (for daily soil water potential) and neutron probes (for volumetric water content every 12 days) across seven stations, with distinct placements for varying irrigation conditions. This comprehensive data, covering topsoil to a depth of 120 cm, verified an approximate 50% reduction in soil moisture for the drought

treatment compared to the control, aiding our evaluation of drought's impact on plant performance and water use efficiency **(Supplemental Figure S1)**. Soil moisture levels were systematically assessed during the 2021/2022 and 2022/2023 field seasons by using two primary techniques: 1) soil water potential was regularly recorded using Watermarks, equipped with remote daily data logging, and 2) volumetric water content was determined using a neutron probe at 12-day intervals (Taylor et al., 2024) (**Supplemental Figure S1**).

The data collected from these sensors, encompassing both topsoil and deeper soil layers, were crucial in monitoring. The significant difference in soil moisture levels was used to assess the impact of drought on crop performance and water use efficiency (**Supplemental Figure S1**).

Core population and sampling

We defined a subsample of unique genotypes that were fully replicated in a randomized complete block design in triplicate in both drought and control treatments, and this population is referred to as the "core population, n = 469 genotypes". However, note that some trees were lost due to mortality in the field **(Supplemental Table 2),** and not all phenotyping was completed in all blocks **(Supplemental Figure S1d-e)**.

For the leaf phenotyping, encompassing stomatal traits and leaf area measurements **(Supplemental Table 1)**, we conducted comprehensive sampling of the core population at two specific time points: June (one month after the drought treatment initiation) and September (106 days after the first collection, which includes an extended period of drought). In June, we sampled all of the core population of the drought treatment (Drought block 1,2,3 n= ~3x469), and in the core population control treatment, we sampled only block 2 (n = 469). Similarly, in September, we sampled the core population in blocks 1,2,3 (n = 3x469) of the drought and only block 2 (n= 469) in control, given time constraints for sampling and analysis. In summary, our analysis encompassed a total of 1,861 trees from both the June and September samplings, comprising 422 unique genotypes (441 trees) from the control group and 468 unique genotypes (1,420 trees) from the drought treatment. For further clarity, please refer to **Supplemental Figure S1c-d**. Wood sampling for carbon isotope discrimination **(Supplemental Table 1)** was performed on the whole “Core” population of all 6 blocks (469 genotypes, n = 3019 samples including replicates) in January 2022.

Climatic data

Climatic data were sourced from WorldClim fit to western North America, which contains a set of global climate layers with high spatial resolution (2.5’), averaging across the years 1970-2000 (Fick & Hijman, 2017). The WorldClim database provides interpolated climate data (a total of 19 variables), including temperature, precipitation, and derived bioclimatic variables, facilitating a comprehensive understanding of the environmental climates of origins for our population of *P. trichocarpa* trees.

Climate variables are the following:

Bio 1 Annual Mean Temperature
Bio 2 Mean Diurnal Range (Mean of monthly (max temp – min temp))
Bio 3 Isothermality
Bio 4 Temperature Seasonality (standard deviation x100)
Bio 5 Max Temperature of Warmest Month
Bio 6 Min Temperature of Coldest Month

Bio 7 Temperature Annual Range
Bio 8 Mean Temperature of Wettest Quarter
Bio 9 Mean Temperature of Driest Quarter
Bio 10 Mean Temperature of Warmest Quarter
Bio 11 Mean Temperature of Coldest Quarter
Bio 12 Annual Precipitation
Bio 13 Precipitation of Wettest Month
Bio 14 Precipitation of Driest Month
Bio 15 Precipitation Seasonality (Coefficient of Variation)
Bio 16 Precipitation of Wettest Quarter
Bio 17 Precipitation of Driest Quarter
Bio 18 Precipitation of Warmest Quarter
Bio 19 Precipitation of Coldest Quarter

Genotypic data

The reference genome and resequencing of the *Populus trichocarpa* population (1,523 genotypes) were conducted by the U.S. Department of Energy Joint Genome Institute (Evans et al., 2014; Tuskan et al., 2006) and are accessible via the Joint Genome Institute Database. We used Genome version: *Populus trichocarpa v4.1, Phytozome genome ID: 533.* Genotypic data were derived from high-coverage whole-genome resequencing. Short reads were aligned to the *P. trichocarpa* reference genome (v3.0) using BWA, with mate pair metadata corrected and duplicate molecules marked using Picard tools. Variants, including SNPs and small indels, were called using SAMtools and bcftools (Evans et al., 2014).

Leaf Sampling

Two fully expanded, first and second mature leaves, specifically the fifth leaf from the apex on each of two south-facing primary branches, were collected at the height of approximately 1.3 m and, lightly misted with water, and sealed in plastic bags and stored in a cooler box on ice. These samples were immediately returned to the laboratory and subsequently kept at 4°C in a refrigerated room. All phenotypic analyses were initiated within 48 hours of collection.

Stomatal Imprinting and Imaging

For the assessment of stomatal morphology, imprints were collected from the right abaxial portion of the leaf section and sampled as previously described (Tricker et al., 2004). A designated rectangular patch of this surface received a coating of clear nail polish. Upon drying, a strip of clear adhesive tape was utilized to lift off a thin layer, capturing a majority of epidermal cells and stomata. The tape was then placed on a microscopic slide and stored until further processing. This methodology resulted in a comprehensive collection of 1,869 imprints of all leaves collected **(example in Figure 1b)**. The imaging phase involved using two Zeiss Standard 16x microscopes, each equipped with camera attachments. All imaging procedures used TCapture software (v5.1.1).

Stomatal Detection and Analysis

To identify stomatal cells in our imprints, we integrated a model rooted in the U-Net architecture conceived within the PyTorch framework. The image data underwent a preliminary preprocessing stage

and was transitioned into tensor format. Using a dataset of 300 representative images for training, our model was meticulously calibrated to distinguish stomatal cells in the imprints efficiently. During the predictive phase, the OpenCV, imported as cv2 (https://pypi.org/project/opencv-python/) software library, facilitated the demarcation of the tightest bounding rectangle around every detected stomatal cell, an integral step for gauging its geometric characteristics. Our analytical process resulted in the calculation of the average stomatal dimensions for each individual imprint (**see example in Figure 1b**).

Leaf area and perimeter

One of the two sampled leaves was used to measure leaf area (LA) and perimeter (PI). We used a Canon EOS Rebel T7i camera positioned over a lightbox (AGPTEK - Model A3USB) to photograph the leaves alongside a scale bar next to the leaves. Subsequently, these images were analyzed further at Oak Ridge National Laboratory (Oak Ridge, Tennessee). In this process, iterative thresholding was applied to the gray-scaled image to separate the lightbox from the rest of the image, from which the leaf segmentation was extracted and rotated to achieve axis symmetry before being cropped to the leaf's bounding box. Once the leaf was distinguished from the petiole, various leaf features, including leaf area and perimeter, were reliably detected and recorded. The analysis was completed using the `scipy` (version 1.11.4) and `scikit-image` (version 0.19.3) libraries in Python.

Dry weight and fresh weight

We measured the fresh weight of one of the two selected leaves, the same leaf that was photographed for the leaf perimeter, area, and fresh weight, using a precision balance (Adam Equipment - PGW 453e). Following this, the leaf was dried for 48 h in a paper bag at 80°C and re-weighed for dry weight. To prevent moisture absorption, all dried leaves were stored with silica desiccant beads.

Contact angle (wettability)

Leaf contact angles were measured as described by (Kwon et al., 2014). A water droplet was placed on the left side of the leaf, while the right side was used for stomatal traits. To initiate the process, we prepared two leaf disks, which were subsequently taped to a microscope slide. For each leaf disk, a distilled water droplet was applied by a pipette. Subsequently, we captured images of the contact surface using a Canon EOS 500D camera. Similar to stomatal detection, we used a convolutional neural network implemented in PyTorch to distinguish water droplets following the region-growing methodology (Lagergren et al., 2023). Using a dataset of 96 images for training and 23 for testing, we achieved a segmentation accuracy (Sørensen-Dice coefficient) of 0.917. Contact angle was measured by fitting a circle to the detected droplets using a Hough transform (Xu et al., 2013), and subsequently measuring the angle of the droplet to the microscope slide (Arnold 2021).

Spectral Reflectance

Spectral reflectance was measured on the adaxial surface of each leaf utilizing a handheld PolyPen RP 410 (Photon Systems Instruments) after samples were returned to the field. The data were subsequently captured and recorded using the SpectraPen software provided by the manufacturer. We used a Spectralon white reference standard to normalize reflectance measurements. From the reflectance spectra, we computed NDVI, defined as Normalized Difference Vegetation Index **(see**

calculations in Supplemental Table 1), and PRI, defined as Photochemical Reflectance Index **(see calculations in Supplemental Table 1)**.

Wood Sampling

Preparation for $\delta^{13}C$

Wood samples for $\delta^{13}C$ analysis were collected in January 2022 from the Core population across all three blocks of both treatments (control and drought), totaling 3019 samples from 479 genotypes. For each sample, three 5-cm segments were harvested from south-facing primary branches at approximately 1.3 m height and stored in labeled paper bags. The samples were dried at 65°C for 14 days to ensure consistent moisture removal.

Following drying, dormant buds at branch tips were carefully removed using shears, while the bark was left intact. The dried wood was ground to a fine powder using a TissueLyser II (Qiagen) with stainless steel grinding jars (2 x 10 ml) at 20 Hz for one minute, yielding a particle size of approximately 0.50 grains per milligram, following a protocol similar to (Moghaddam et al., 2013). Ground samples were transferred into labeled plastic vials, and precisely 3 mg (±10%) of powder was measured into tin capsules, which were folded as necessary for analysis. The capsules were arranged in 96-well plates, with two duplicates included in each of the 33 plates.

The prepared samples were sent to the UC Davis Stable Isotope Facility for carbon isotope discrimination analysis using Isotope-Ratio Mass Spectrometry (IRMS).

Calculations of δ13C

The following was used to calculate δ13C:

$$\delta 13C = \ ((13C/12C)standard)/(13C/12C)sample)\ x\ 1000‰$$

This value is expressed in parts per thousand (‰) and compares the ratio of 13C to 12C in the sample to that in a standard (typically a belemnite formation from the Peedee Formation in South Carolina, known as PDB). A negative δ^13C value implies that the ^13C/^12C ratio in the plant is lower than that in the standard. Since plants discriminate against d13C, most plants have negative δ^13C values. The more negative the value, the stronger the preference for ^12C in the photosynthetic process. A higher WUE is indicated by a higher ^13C/^12C ratio (less negative δ^13C values and less discrimination against ^13C).

Tree height

Biomass productivity data were collected as tree height measurements in March 2021 (beginning of the growing season, after leaf flush) and November 2021 (end of growing season, after bud set), following the first year of the applied drought treatment. The height of every experimental tree across each block of both treatments was recorded using a telescopic height pole.

Statistical analysis

Statistical analyses were performed using RStudio (v4.1.2). We visualized spatial data using the Leaflet package (v1.7.1), a JavaScript library for interactive maps. After loading the necessary library, our geospatial data was overlaid on a CartoDB Positron basemap on which the data points can be placed. During the data exploration and organization phases, we employed a suite of packages including “dplyr”, “tidyverse”, “tidyr”, “plotrix”, “data.table”, and “stringr”. Enhanced data visualization was achieved with the “ggplot2” package, facilitating the creation of frequency diagrams, reaction norms, and boxplots. For statistical significance testing and Analysis of Variance (ANOVA), we utilized packages such as “stats”, “lme4”, “emmeans”, and “lmerTest”."

Water content

The Water content was calculated using the fresh weight and dry weight of leaf samples.

The water content (WC) was also calculated by using (**see Supplemental Table 1)**:

$$WC = \ (fresh\ weight\ (g) - dry\ weight\ (g))$$

Proportional water content (PWC) was also calculated by using (**see Supplemental Table 1)**:

P$WC = \ (fresh\ weight\ (g) - dry\ weight\ (g))/fresh\ weight$ (g)

Drought response

To quantify the plasticity of the trait, we employed the formula:

$$Drought\ plasticity\ Index = \ (Mean\ Trait\ Value\ under\ Control - \ Mean\ Trait\ Value\ under\ Drought)$$

This index provided a relative difference value, representing the extent of trait variation due to drought exposure across different genotypes **(Figure 2B).**

Drought Resilience index (DRI)

$$DRI = \ (phenoD/phenoC)/(mean\ phenoD/mean\ phenoC)$$

$phenoD$ = Phenotype drought
$phenoC$ = Phenotype control
$mean\ phenoD$ = population mean of Phenotype D
$mean\ phenoC$ = population mean of Phenotype C

This index calculates the ratio of yield reduction under stress in a specific genotype relative to the average reduction across all genotypes **(Supplemental Table 4).** PhenoD refers to a phenotype of the drought treatment, and phenoC refers to a phenotype of the control treatment.

Relative growth rate

The relative growth rate of height was calculated with this equation:

RGR= $(\ln(W_2)-\ln(W_1))/(\ln\ (W_1))$
where:
W_1 represents the height taken in March of 2021.
W_2 represents the height measured in November of 2021.

Estimating correlations and variance components of traits

To estimate the relationships between plant traits, pairwise Pearson correlation coefficients were calculated separately for control and drought treatments in R with cor(..., use="complete.obs"). These correlations were visualized with a heatmap in R.

In our analysis, the contribution of Genotype (G), Treatment (T), and their interaction (G:T) to the variance in plant traits was estimated. This estimation was conducted in R, utilizing the lme4 package, where Genotype, Treatment, and Interaction were treated as random effects. Post-model fitting, the variance components were extracted using the VarCorr function, and the variance associated with Genotype, Treatment, Interaction, and Residual were isolated. The total variance was computed as the sum of these components. Subsequently, the percent variance explained by each component was calculated by dividing each variance component by the total variance and multiplying by 100.

Model:
$y_{ijk}=\mu+G_i+T_j+(G\times T)_{ij}+\epsilon_{ijk}$

where:
y_{ijk} represents the observed trait value for the ith genotype, jth treatment, and kth observation.
μ is the overall mean of the trait across all genotypes and treatments.
G_i represents the random effect of the ith genotype.
T_j represents the fixed effect of the jth treatment.
$(G\times T)_{ij}$ is the random interaction effect between the ith genotype and jth treatment.
ϵ_{ijk} denotes the residual error term associated with each observation, capturing the variability not explained by the other components in the model.
The percent variance explained by each component is calculated as:

$$\%VarianceComponent = \ (VarianceComponent/Total\ Variance)x100$$

Estimation of broad sense heritability for traits and genetic correlation.

An upper limit of broad-sense heritability, which is clonal repeatability, for a total of 30 traits were calculated by estimating genetic variance as per the below univariate model.

$$y = 1\mu\ + Zg + e$$

$$g \sim N(0, \sigma_g^2 I);\ e \sim N(0, \sigma_e^2 I)$$

$$H_R^2 = \frac{\sigma_g^2}{\left(\sigma_g^2 + \sigma_e^2\right)}$$

Here ***y*** is an (*n*×1) vector of transformed trait values for all ramets (*n*) for a given trait in either drought or control treatment. The trait mean is denoted by μ and **1** is a (*n*×1) vector of ones. The vector **g** is a (*i*×1) vector of total genetic effects for *i* individual genets, modelled by the (*n*×*i*) incidence matrix ***Z*** and σ_g^2

represents the total genetic variance. ***e*** is an (n×1) vector of random residuals and σ_e^2 is its variance estimate.

I represents an identity matrix of corresponding dimensions and ignores the relatedness among genets when modelling ***g***. The following bivariate model was used to estimate trait-trait covariance for each pair of traits thus making it possible to calculate pair-wise genetic correlation (r_g).

$$\begin{bmatrix} \boldsymbol{y_{t1}} \\ \boldsymbol{y_{t2}} \end{bmatrix} = \begin{bmatrix} \mathbf{1}_{(n\times 1)} & \mathbf{0}_{n} \\ \mathbf{0}_{n} & \mathbf{1}_{(n\times 1)} \end{bmatrix} \begin{bmatrix} \mu_{t1} \\ \mu_{t2} \end{bmatrix} + \begin{bmatrix} \boldsymbol{Z_{t1}} & \mathbf{0}_{(n\times i)} \\ \mathbf{0}_{(n\times i)} & \boldsymbol{Z_{t2}} \end{bmatrix} \begin{bmatrix} \boldsymbol{g_{t1}} \\ \boldsymbol{g_{t2}} \end{bmatrix} + \begin{bmatrix} \boldsymbol{e_{t1}} \\ \boldsymbol{e_{t2}} \end{bmatrix}$$

$$\begin{bmatrix} \boldsymbol{g_{t1}} \\ \boldsymbol{g_{t2}} \end{bmatrix} \sim \mathbf{N}(\mathbf{0}_{(2i\times 1)}, \boldsymbol{T}^*)$$

$$\boldsymbol{T}^* = \mathbf{T} \otimes \boldsymbol{I}$$

$$\boldsymbol{T} = \begin{bmatrix} \sigma_{t1}^2 & \sigma_{t1t2} \\ \sigma_{t1t2} & \sigma_{t2}^2 \end{bmatrix}$$

$$r_g = \frac{\sigma_{t1t2}}{\sqrt{\sigma_{t1}^2} \times \sqrt{\sigma_{t2}^2}}$$

Here, y_{t1} and y_{t2} are (n×1) vectors with trait values for the pair of traits under consideration (t_1 and t_2) while μ_{t1} and μ_{t2} are means for each trait respectively. $\mathbf{g}_{t1}$ and $\boldsymbol{g}_{t2}$ represent (i×1) vectors of total genetic values for t_1 and t_2 respectively modelled by the (n×i) $\boldsymbol{Z}_1$ and $\boldsymbol{Z}_2$ incidence matrices. Covariance of genetic values were modeled by $\boldsymbol{T}^*$ and was obtained as the Kronecker product (⊗**)** between ***I*** and ***T*** matrices. For both univariate and bivariate models described above, solving linear mixed model equations, obtaining REML estimates of variance covariance components and obtaining standard errors of statistics were carried out as per methods described in (Lynch & Walsh, 1998) and implemented in (Covarrubias-Pazaran, 2016).

Climate-Trait Correlations

For assessing relationships between traits (separately for drought and control treatments) and climate of origin (Bioclimatic variables 1-19 from WorldClim) of experimental trees, Spearman's rank correlation coefficient was computed using R. The Spearman's correlation measures the strength and direction of monotonic associations between paired data. This non-parametric test was chosen due to its robustness against outliers and its capability to detect non-linear relationships. Calculations were performed using the cor.test() function with the method set to "spearman" from the base R package.

Random forest prediction of traits in relation to climate of origin

Utilizing the Random Forest package in R, we implemented a random forest regression model to analyze the impact of climate on INT trait values under drought conditions, informed by 19 WorldClim Bioclimatic variables. Our models, each comprising 500 trees, were validated to ensure convergence, confirming additional trees would not enhance predictive accuracy. The model's efficacy was assessed by comparing observed and predicted trait values. We then plotted the predicted values from the resulting random forest model for traits across the range of *P. trichocarpa* to visualize the geographical patterns of traits and climate.

Genome-wide association studies (GWAS)

Trait values and genotype means were transformed using a rank-based inverse normal transformation (INT) following (Auer et al., 2016). This transformation standardizes genotype values to improve normality, reducing skewness and enhancing both statistical power and interpretability for downstream analyses. Genome-wide associations were conducted for all traits using genotype means for drought, control treatments, and their plasticity. Genomic variation, including single nucleotide polymorphisms (SNPs) and small insertions/deletions (InDels), was obtained from previous research (Tuskan et al., 2006; Evans et al., 2014). Associations between genome-wide genetic variants and phenotypic traits were analyzed using GEMMA (v0.98.4) (Zhou & Stephens, 2012), incorporating a kinship matrix as a random covariate to account for population structure. Each genetic variant was modeled using the equation $y=X\beta+g+\epsilon$, where y is the vector of trait values for each individual, X is the matrix of fixed effects (variants), β is the vector of fixed-effect coefficients, g represents the random genetic effect due to population structure and relatedness, and ϵ is the vector of residual errors. The statistical significance of allele-trait associations was determined by the p-value of β. Variants were filtered to include only those with a minor allele frequency (MAF) ≥ 0.05. To identify putative GWAS peaks and address redundancies caused by linkage disequilibrium (LD), alleles were clustered using PLINK with parameters: --clump-p1 1, --clump-p2 1, --clump-r2 0.05, and --clump-kb 50. The 50-kb clumping threshold was informed by the genome-wide LD decay rate, which reached equilibrium at an r^2 of 0.05 within a 50-kb window. This process identified the most statistically significant allele for each LD group.

For visualization, clumped alleles were initially filtered to retain those with $p<1\times10^{-4}$. Further refinement was performed based on a Bonferroni-corrected significance threshold ($p\leq0.05$) using a chi-squared test to evaluate the significance of all linked alleles within each clump against a uniform p-value distribution. Genes located within 20 kb of the most significant variant in each clump were selected for downstream analyses. We visually inspected qqplots to confirm adequate control for population structure **(Supplemental Figure S5).**

Putative paralogs of *Arabidopsis thaliana* genes (TAIR10) in the *P. trichocarpa* proteome were identified using BLASTP (BLAST 2.13.0+) with the following criteria: E-value < 1×10−5, bitscore > 100, and percent identity > 30%. For each *P. trichocarpa* protein, the *A. thaliana* gene with the lowest E-value was retained. We then checked the gene descriptions and gene ontology (GO) annotations for terms such as “stomata,” “water,” “guard cell,” and “abscisic acid” to identify candidate genes associated with these processes. From this, we generated lists of loci (available in Supplemental Table 7) for future research aimed at identifying potential causal loci. The number of times each gene was located within 20 kb of a GWAS signal associated with traits was also recorded to guide further exploration.

Elucidating the Role of Chromosome 10 Locus in Stomatal Size

We examined, in greater detail, a locus on Chromosome 10 consistently associated with stomatal size under both drought and control treatments and at two measurement time points. The pronounced signal from this locus provided a unique opportunity for an in-depth case study, aiming to answer several pivotal questions:

To assess the LD across this genomic window, we calculated the Pearson correlation between all variant pairs in this 20 kb window, subsequently visualizing the results in a heatmap format and by visualizing LD with the most significant variant. Utilizing a random forest model (implemented in R using the randomForest package, with 500 trees), we modeled trait~climate relationships based on genotypes with known phenotypic data. This model enabled us to predict stomatal size for genotypes with previously unmeasured traits based on their climate of origin, employing bioclimatic variables sourced from WorldClim 2.0. We then assessed the predicted allele effects by examining these predicted phenotypes with the respective allele states across our dataset

Lastly, we investigated the relationship between allele state and climatic variables. This entailed calculating the t-statistic for the correlation between allele states and each individual bioclimatic variable. Furthermore, we employed a random forest model, incorporating all bioclimatic variables to predict allele states. The accuracy of this model was gauged through analysis of the confusion matrix in R. Predicted allele states were projected and mapped across the geographical range of *P. trichocarpa*.

Future climate predictions of Chromosome 10 locus

To investigate the potential impact of future climate changes on the frequency of a specific allele associated with stomatal size on chromosome 10, we employed high-resolution future climate projections and predictive modeling. This allele was selected based on its significant association to stomatal size and with the climate of origin, suggesting its potential responsiveness to future climatic shifts. We utilized downscaled future climate projections (10-minute spatial resolution) from the Coupled Model Intercomparison Project Phase 6 (CMIP6), available through WorldClim version 2.1, which, as described (https://www.worldclim.org/data/cmip6/cmip6climate.html), underwent both downscaling and calibration (bias correction) against the baseline climate provided by WorldClim v2.1 Our analysis encompassed data from ten global climate models (GCMs), specifically: ACCESS-CM2, CMCC-ESM2, EC-Earth3-Veg, GISS-E2-1-G, INM-CM5-0, IPSL-CM6A-LR, MIROC6, MPI-ESM1-2-HR, MRI-ESM2-0, and UKESM1-0-LL. We evaluated these models across four Shared Socio-economic Pathways (SSPs): SSP1-2.6, SSP2-4.5, SSP3-7.0, and SSP5-8.5, at four future time intervals: 2021-2040, 2041-2060, 2061-2080, and 2081-2100.

Initially, we compared future climate predictions to current climatic conditions (baseline) using bioclimatic variables from WorldClimat the geographic locations of *P. trichocarpa* genotypes with t-tests, using T-test statistic as a unitless measure of the severity of change for each bioclimatic variable. This preliminary step established an understanding of the extent of future climatic changes potentially facing *P. trichocarpa*.

To predict future allele frequencies, we adopted a machine learning approach using random forest models in R. This involved analyzing the single nucleotide polymorphism (SNP) with the strongest correlation to stomatal size within the identified locus on Chromosome 10. Given the imbalanced genotype frequencies, we first balanced the dataset through random downsampling. From this balanced dataset, we trained a random forest model to predict genotype frequencies based on bioclimatic variables. This model was applied to both the current climate baseline and all future climate scenarios for each combination of GCM, SSP, and time interval.

To ensure robustness, this process was iterated 100 times with random downsampling to obtain balanced training datasets, resulting in a total of 16,000 model predictions. For each prediction, we calculated the frequency of the allele associated with smaller stomata and compared it to the baseline frequency predicted from current climate conditions.

RNA-Seq Data Generation and Differential Expression Analysis

RNA extraction, library construction, and sequencing were conducted following the protocols described by (J. Zhang et al., 2018). Sequencing was performed on the Illumina HiSeq 2500 platform using paired-end 150-bp reads. The dataset, including NCBI SRA accession numbers for publicly available sequences, is detailed in **Supplemental Tables 8 and 9.**

Differential expression analysis was conducted to identify genes associated with stomatal size by comparing genotypes within the top 10% ("big" stomata) and bottom 10% ("small" stomata) quantiles. Raw RNA-Seq count data were processed using DESeq2 (Love et al., 2014) in R. Genes with low expression (total counts ≤ 1 across all samples) were filtered out to enhance statistical power.

Significant differentially expressed genes (DEGs) were identified using an adjusted p-value (padj) $\leq$ 0.05 and an absolute log2 fold change (|log2FC|) ≥ 1. Gene annotations were integrated by mapping significant DEGs to the *Populus trichocarpa* genome (v3.1) for functional insights. Results were visualized using volcano plots generated with ggplot2, highlighting the relationship between fold changes and statistical significance.

Results

Drought implementation and trait responses

We imposed drought and irrigated treatments on field trials of diverse *P. trichocarpa* during the summer of 2021 in Davis, California (**Figure 1, Supplemental Figure 1**). The successful implementation of water limitation was confirmed by regular measurements of soil water potential and the lack of precipitation during the treatment period (**Supplemental Figure 1).** Total precipitation recorded from June to September 2021 was 0.51 mm. The effect of water deficit was visually evident in *P. trichocarpa* trees, such as wilting or yellowing leaves and early leaf shedding in the drought-treated trees. The effect of drought relative to control conditions was detected in a number of traits measured **(Supplemental Table 1, Supplemental Table 2, Supplemental Table 3, Supplemental Table 5)**, especially those traits related to biomass and performance. Drought treatment significantly reduced leaf size, leaf mass, height, and growth rate (**Figures 2 and 3)**. Among leaf morphological traits, we saw a significant trend for smaller, more dense stomata under drought conditions along with reductions in specific leaf area, leaf perimeter, and abaxial contact angle, reflecting constraints on growth, and whether the plasticity is adaptive remains a question for future work **(Figures 2 and 3).** Notably, water-related traits, $\delta^{13}C$, a proxy for water-use efficiency, were significantly higher under drought, suggesting a water conservation response. For traits where measurements were made at multiple time points, the effect of drought was more pronounced on measurements made in September, after several months of water deficit, than in June, shortly after the onset of the drought treatment **(Figures 2 and 3)**. This is especially clear in spectral

reflectance data. For example, the difference between control and drought for PRI and NDVI was most evident in September. In particular, PRI was dramatically reduced in drought-treated plants, indicative of physiological stress (Magney et al., 2016; Mulero et al., 2023; Wong et al., 2022).

Trait correlations were similar under drought and control treatments (**Figure S4**). Positive correlations were observed between Stomatal Size in June and Stomatal Size in September, indicating consistency in trait behavior across different growth stages and durations of drought (June vs. September). A negative correlation was evident between Stomatal Density and Stomatal Size, consistent with previous observations in poplar (McKown, Guy, Klápště, et al., 2014) and other species (Franks et al., 2009; C. Liu et al., 2021). We also observed significant plasticity in several traits. The variance components analysis from the experimental field trial delineated variability in plant traits into three sources: Genotype (G), Treatment (T), and their interaction (GxT). Genotypic variance was observed across most traits, underscoring the significance of genetic differences among the samples (**Supplemental Figure S2**). Environmental treatments significantly affected traits such as Stomatal Size in September and Leaf Compactness in June. The interaction between genotype and treatment was evident in traits such as Water Content, indicating a differential response of genotypes to various treatments. Overall, the findings emphasize the complex interplay of genetics and environment in determining plant trait variability, in particular, in response to drought.

For the drought treatment, where replication allowed such analyses (see Materials and Methods), all traits showed significant clonal repeatability (H2R) except for adaxial contact angle, a proxy for wettability, for the time point measured in September (**Figure S3a**). As expected, we observed high genetic correlation (rG) for traits across June and September (**Figure S3b**). Leaf biomass traits (perimeter, dry and fresh weight) showed high positive rG with each other and were significantly negatively correlated with specific leaf area. Interestingly rG was strongly negative between adaxial and abaxial contact angle indicating possible trade-offs between these traits. Furthermore, adaxial contact angle was strongly negatively correlated with leaf biomass traits, relative water content, relative growth rate, NDVI and PRI. As also seen with phenotypic correlations, stomatal density and stomatal size showed strong negative rG.

Relationships between Traits and Climatic Conditions

We found significant correlations between plant traits and the climate of their origin **(Figure 3)**. Greater leaf size and weight, for instance, were predominantly associated with cooler, wetter climates. Notably, stomatal density and size demonstrated contrasting relationships to climatic conditions. Specifically, genotypes originating from warmer, arid climates exhibited higher stomatal densities but possessed smaller stomatal sizes. Warmer, drier climates correlated with less negative δ13C (water use efficiency) values. To provide a more nuanced understanding of the interaction between climatic variables and plant phenotypes, we employed Random Forest (RF) models (**Figure 3b-d)**. The strength of RF models lies in their ability to detect non-linearities and interactions, thereby potentially enhancing the accuracy of predictions. Nevertheless, they do present challenges in terms of interpretability for targeted hypothesis testing. These RF models confirmed a marked correlation between the predicted values and the actual measurements. Visualizing these predictions across the range further emphasized the relationships between stomatal size, geography and climate.

Genome-Wide Associations (GWAS)

We performed GWAS analyses for each trait: phenotypes under drought, control, and the difference (plasticity) **(Supplemental Figure S5-7, Figure 5, Supplemental Tables S5 and S6)**. These analyses identified loci explaining variance in traits after accounting for population structure. In total, across all traits, environments and plasticity, we identified 303 significant associations, each reflecting a cluster of SNP variants in linkage disequilibrium enriched for association to the trait of interest.

Evaluating GWAS results across traits after variant climping and considering multiple testing revealed a notable locus on Chromosome 10. This region was significantly associated with stomatal size in both drought and control treatments, and for measurements in both June and September, as well as for abaxial contact angle, a proxy measure of cuticle wax (**Figure 4, Supplemental Figure S6 and S7)**. We found that alleles in this locus explained 15.9% of the variance in stomatal size across all measured plants, irrespective of treatment. This region contains a cassette of tandem 3-ketoacyl-CoA synthase (KCS) family genes, with KCS genes being previously linked to both cuticular wax and stomatal traits (Gonzales-Vigil et al., 2017; Gray et al., 2000). A KCS gene in this region was previously linked to high alkene content in abaxial cuticular wax and differences in stomatal size in *P. trichocarpa (Gonzales-Vigil et al., 2017)* and may also be linked to Melampspora and Septoria resistance (pers. com). The linkage disequilibrium around this region revealed that the variants with strong associations had significant long range LD with one another, consistent with a solitary causal locus with extensive LD with neighboring variants **(Supplemental Figure S7**).

For more mechanistic insight into variation in stomata size, we used a bulk segregant RNA seq analysis from leaf tissue **(Supplemental Table 8)**. We identified 51 genes differentially expressed between the top and bottom deciles of genotypes ranked by stomata size. Only one of these genes co-localized with a GWAS signal: Potri.010G079500, which showed a >4-fold difference in expression ($p=7.35x10^{-5}$, adjusted p=0.046), one of the KCS genes on Chromosome 10 adjacent to the most significant GWAS signal for stomata size (**Figure 4c**), providing further evidence for the causal link between variation in KCS genes and stomatal size.

To explore its role in local adaptation to climate, we estimated allele effects on climate-predicted phenotypes for *P. trichocarpa* genotypes whose stomatal phenotypes were not analyzed in this study **(Figure 5)**. The rationale behind this approach was multi-fold. Primarily, it served as a strategy to verify the integrity of climate-trait associations. If the phenotype predictions based on climate were accurate and reflect local adaptation, they should replicate the empirical allele effects observed in genotypes for which phenotypes were measured. Secondly, it showcases the potential of leveraging local adaptation in employing climate-predicted phenotypes in a broader genotype sample to augment efforts in pinpointing physiologically significant loci. These analyses are in essence a form of environmental GWAS which treat environment of origin as a phenotype, (e.g., (Ferrero-Serrano & Assmann, 2019). In our case because the predicted phenotype is derived entirely from climate of origin, it reflects a transformation of the environmental parameters fit to a target trait, thereby potentially enhancing the study of locally adaptive alleles.

These analyses confirmed that observed allele effects were highly predictive of allele effects on phenotypes predicted by climate of origin in unmeasured genotypes (stomatal size: $r = 0.95$, $p<2x10^{-16}$**)**. Examining the most significant SNP within this region yielded two noteworthy findings: an observable additive effect where heterozygous individuals presented an intermediate phenotype and a match between the empirical "effect" and climate-predicted phenotypes **(Figure 5)**. Further exploration into climate-allele associations revealed that alleles linked with small stomata were predominant in

environments characterized by reduced warm-season precipitation and greater precipitation seasonality **(Figure 5d, Supplemental Figure S8)**. This aligns with the general trait correlations we noted, consistent with the distribution of alleles at this locus reflecting local adaptation to climate. The robustness of the relationship between the climate and allele state is further emphasized when predicting the allele state using the random forest model based on climate parameters (X^2 test, $p<2x10^{-16}$, **Figure 5)**.

Future climates

Given the strong link between loci affecting stomata size and climate, we set out to ask whether this yields predictions about future evolution at this locus. We evaluated the severity of climate change across various bioclimatic variables at the geographic locations of *P. trichocarpa.* These were based on different Shared Socio-economic Pathways (SSPs) and temporal projections, revealing that more intense SSP scenarios forecasted more substantial changes in climate, intensifying over time (**Figure 5 g and i**).

As expected, the predicted changes in climate suggest a general trend toward warming. Notably, there is an expected increase in the extremities of precipitation - wetter conditions during the colder months coupled with drier conditions throughout the summer months. These shifts in temperature and precipitation patterns may drive natural selection on stomatal size. The allele associated with smaller stomatal size is found to be more prevalent in environments with high intra-annual precipitation variability and drier summer months—conditions that are expected to become more common in the future for *P. trichocarpa* (**Figure 5g and h**).

Our predictive models, averaging across all 10 Global Climate Models (GCMs) for each set of 100 random iterations, indicated a predicted increase in the expected frequency of the small stomata allele, particularly under the more severe climate scenarios (SSP3-7.0 and SSP5-8.5), with a notable escalation over time **(Figure 5g and h)**. These increments were most pronounced in the latter half of the 21st century. Taken together, these findings support the hypothesis that allelic variation associated with stomatal size reflects local adaptation to climate, which may be perturbed by extreme climate change.

Discussion

This study has identified novel genetic loci that underpin phenotypic variation in stomatal and other leaf traits linked to*P. trichocarpa* crop adaptation to future water-limited environments. These findings will be informative in enabling future feedstock development for marginal environments. By deploying a controlled drought experiment, subjecting over 7,000 trees across 6.1 ha to a controlled soil moisture deficit, we have begun to unravel the complexities of adaptive versus plastic responses to drought. Our findings provide evidence for local adaptation in *P. trichocarpa*, with associations between climate and functional traits (Viger et al., 2016).

We estimated the genetic variance of drought-related traits using broad-sense heritability (H2R), an upper-limit estimate of the proportion of total genetic variance to phenotypic variance. Control block estimates were not possible due to single ramet measurements per genet. SNP-heritability results were similar to H2R, suggesting overestimation of additive genetic values, likely due to low relatedness among genets causing the genomic relationship matrix (GRM) to approximate an identity matrix. While we couldn't fully separate additive from non-additive genetic effects, estimates of genetic correlations (rG) provided key insights.

Stomatal size and density showed high heritability and a strong negative genetic correlation, consistent with their functional trade-off under water-use efficiency constraints. This trade-off has been observed across other tree species and validated through genetic manipulation in Arabidopsis. Leaf traits like PRI and NDVI, which are indicative of light absorption processes, also showed strong negative genetic correlations with adaxial contact angle and most leaf biomass traits. Lower adaxial contact angle indicates increased wettability, which could reduce gas exchange and carbon assimilation. These observed correlations suggest that leaf morphology and associated indices may reflect adaptive mechanisms under drought stress in our plantation setting.

Our analysis indicates that stomatal traits are closely linked to the climatic conditions of their geographic origin, with genotypes from hotter, drier climates often exhibiting smaller, denser stomata, consistent with previous findings (Pearce et al., 2006). This relationship is valuable for considering poplar as a bioenergy crop in marginal lands and could help inform the selection of genotypes with stomatal traits and other traits aligned to the target environment of production. The plastic response of stomatal size reduction under drought conditions may reflect an adaptive response, supporting smaller stomata associated with arid environments and underscoring their role in optimizing water-use efficiency (Dunlap & Stettler, 2001). No strong relationship between stomatal size and height or RGR (**Figure S4**) was observed, indicating that these traits can be disentangled, enabling future selection and breeding of adaptive stomatal traits for hot and dry environments, with maintained yield. While WUE increased under drought, potentially reflecting adaptive plasticity, a relationship with stomata size was not evident.

We identified a significant locus on Chromosome 10 associated with stomatal size and abaxial contact angle, showing a distribution among genotypes highly predicted by the climate of origin. A significant locus on chromosome 10 was previously found to be important in determining δ13C in a bi-parently mapping population with one grandparent as *P. trichocarpa* (Viger et al., 2013), thus linked to plant WUE. Of the known candidates that map to this Chromosome 10 locus, 3- Ketoacyl-COA synthase 11, KCS11 is a gene family member involved in the biosynthesis of Very Long Chain Fatty Acids (VLCFAs) codes for long-chain fatty acids, already shown to have a role in stomatal development and function in relation to drought tolerance and stomatal response to elevated carbon dioxide (Gray et al., 2000; Tang et al., 2020). Future work will benefit from the availability of long-read sequence data to capture potential structural variants and long-range haplotypes that characterize the variation in this region for greater causal inference. This could prove a promising candidate for genetic exploration to enable precise gene editing (Allwright & Taylor, 2016; Taylor et al., 2019, 2024). Investigating this and other loci could reveal causal variants, providing breeders with tools to develop *Populus* varieties tailored for specific environmental demands. This approach aligns with sustainable biofuel production goals and broader environmental stewardship efforts. However, detailed mapping of these regions is necessary to unravel underlying genetic mechanisms (**Supplemental Table 7**). Presently, these genetic markers identified provide a resource for future studies aiming to dissect the genetic basis of adaptation in *P. trichocarpa*.

P. trichocarpa's current adaptation to its climate underlines the need to explore resilience under changing future climates, since the ability to predict alleles with future adaptive value is essential for conservation and the management of natural populations (Blumstein et al., 2020). The adaptability shown by *Populus balsamifera*, through a wide range of adaptive physiological responses, offers hope for potential resilience against future climate shifts (Keller et al., 2011). The clinal variation and genomic signals observed in *P. trichocarpa* indicate a blend of unique and shared adaptive responses to different environmental gradients, shaped by genomic, environmental, and functional factors (M. Zhang et al.,

2019). Such insights lay a groundwork for understanding adaptation mechanisms in species facing climate change threats.

Predicting stomatal size from the climate of origin offers an approach to inferring phenotype values in genotypes without direct measurements, aiding in the association between observed alleles and traits. This methodology holds the potential for streamlining the assessment of complex physiological traits, though its applicability across various traits and species requires more empirical validation. We found novel evidence of predicted allele frequency shifts towards those associated with smaller stomatal size under future climate projections, especially under severe scenarios, suggesting that natural selection may favor traits conducive to surviving anticipated shifts in precipitation patterns **(Figure 5)**. This trend prompts crucial considerations about the pace of evolutionary dynamics in perennial species like *P. trichocarpa* in response to forecasted rapid environmental changes and the implications for the species' persistence and resilience. In contrast, for research on conifer trees, there is evidence of limited adaptation to local climate for populations of Douglas-ir (Candido-Ribeiro & Aitken, 2024) although this study largely considered photosynthetic traits only and is in contrast to earlier research on Douglas-ir that demonstrated significant intraspecific population variation in traits in relation to climate of origin (Bansal et al., 2015), or relevance to identifying adaptive and plastic responses to enable drought tolerance in the face of climate change. For *P. trichocarpa,* our data suggest significant need for allele frequency shifts with climate, but the timing and importance of these phenomena require further investigation

While our findings provide valuable insights into loci and traits associated with drought tolerance, it is critical to acknowledge the inherent trade-off between drought tolerance and yield. Resources allocated to survival mechanisms under stress conditions often come at the expense of growth performance, particularly over multiple years. Breeding strategies must carefully navigate this balance to develop genotypes capable of both surviving extreme conditions and maintaining productivity. The loci identified in this study offer a promising foundation for achieving this balance, but long-term evaluations under variable environmental conditions are needed to fully understand their implications.

Utilizing natural populations preserves biodiversity and reduces the long breeding cycles typical of forest trees by maintaining allele-phenotype relationships. While marker-assisted selection often struggles with complex traits, genomic selection, leveraging genome-wide markers to predict traits beyond known climatic envelopes, offers significant potential for adaptive breeding strategies under climate change (Cortés et al., 2020; Depardieu et al., 2020; Grattapaglia et al., 2018). Additionally, our research supports identifying single gene targets for gene editing, as demonstrated in Populus ((Zhou et al., 2015)), accelerating wood domestication ((Anders et al., 2023)).

Poplar is a fast-growing, short-rotation crop with diverse applications, including Sustainable Aviation Fuel (SAF) production (Webber et al., 2024).

. Bioenergy with Carbon Capture and Storage (BECCS), and other bio-based uses, making it a cornerstone of sustainable energy strategies ((Porth & El-Kassaby, 2015; Sannigrahi et al., 2010)). This versatility emphasizes the importance of breeding programs aimed at improving efficiency, yield, and adaptability, particularly on marginal, water-limited sites—a key limitation for bioenergy crop deployment ((King et al., 2013)). Together, these approaches can optimize woody feedstocks for future climates while addressing the critical trade-offs between drought tolerance and yield. This aligns with the U.S. Department of Energy goals to triple biomass supply and meet 15% of energy demand through sustainable bioenergy crops (U.S. Department of Energy, 2024)). By addressing these gaps, our work

advances conservation and breeding strategies for poplar and other species, supporting its diverse applications in a changing global climate.

Conclusion

We have uncovered evidence of adaptive variation in stomatal and leaf traits within *P. trichocarpa*, pinpointing a set of loci associated with genetic variation under both drought and control conditions, as well as their plasticity. Our findings also underscore the critical role of climate in shaping the adaptive landscape of *P. trichocarpa*, casting light on potential challenges and opportunities for this species in the face of climate change. Leveraging climate-predicted phenotypes provided compelling evidence for the adaptive significance of a locus associated with stomata size, which is predicted to respond to selection under future climates. In summary, this work offers pivotal insights into the intricate genetic underpinnings of physiological traits and their drought responses in *P. trichocarpa,* with implications for both conservation strategies and breeding initiatives.

Acknowledgments

This research was conducted on the ancestral land of the Patwin people. University of California, Davis land acknowledgment statement: https://diversity.ucdavis.edu/land-acknowledgement-statement
Furthermore, we thank all UC Davis interns, graduate students, and postdocs who helped with field collections and lab assistance on this project.

Funding

This research is supported by the Center for Bioenergy Innovation (CBI), U.S. Department of Energy, Office of Science, Biological and Environmental Research Program under Award Number ERKP886. Research in the laboratory of Gail Taylor is supported by the John B. Orr endowment in Environmental Plant Sciences and this project was supported by the Genomics-Enabled Plant Biology for Determination of Gene Function program by the Office of Biological and Environmental Research in the DOE Office of Science (award DE-SC0020164).
MCK acknowledges the Department of Plant Sciences, UC Davis, for the award of a GSR scholarship funded by endowments, particularly the James Monroe McDonald Endowment, administered by UCANR.

Conflict of Interest

The authors declare no conflict of interest.

Data availability

All included.

Figures

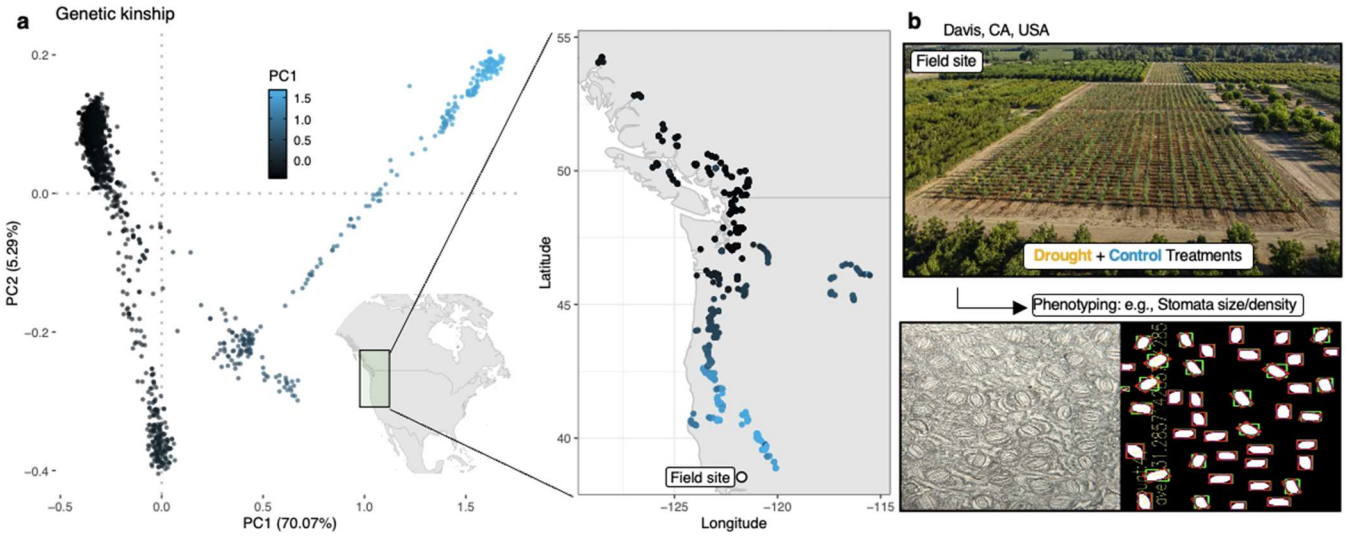

Figure 1. Overview of population and experiment. (a) Principal components of genetic kinship among *Populus trichocarpa* genotypes and their location of origins in the Pacific Northwest. **(b)** Common garden location and an example of stomatal phenotyping. On the left: raw microscopy image; on the right: processed image suitable for identifying stomatal density and size, captured at 16x magnification.

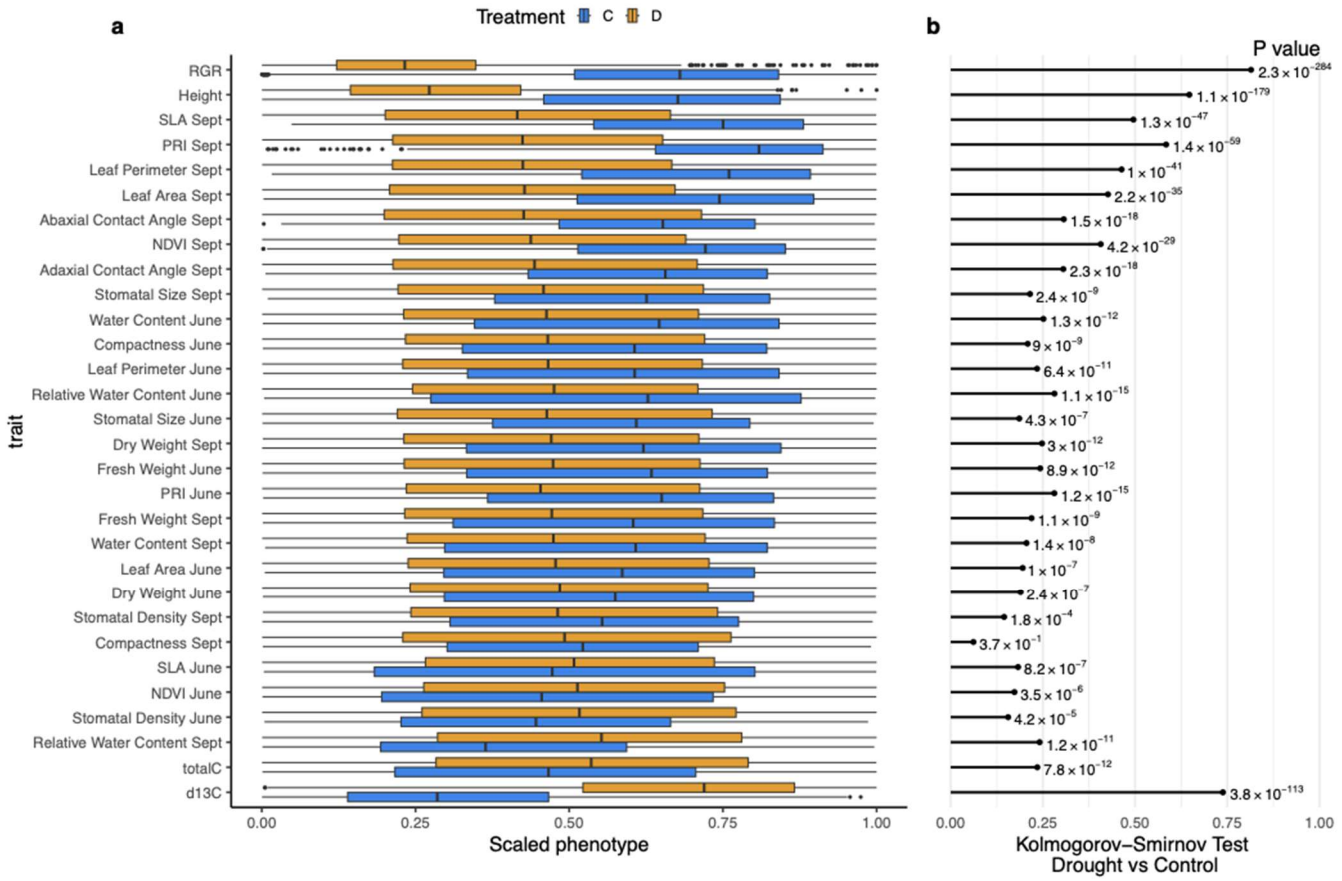

Figure 2. Phenotypic responses to drought and control treatments. (a) INT scaled phenotypes for traits under control (C, blue) and drought (D, orange) treatments. (**b)** Kolmogorov–Smirnov test statistic and corresponding P-values comparing trait distributions between treatments.

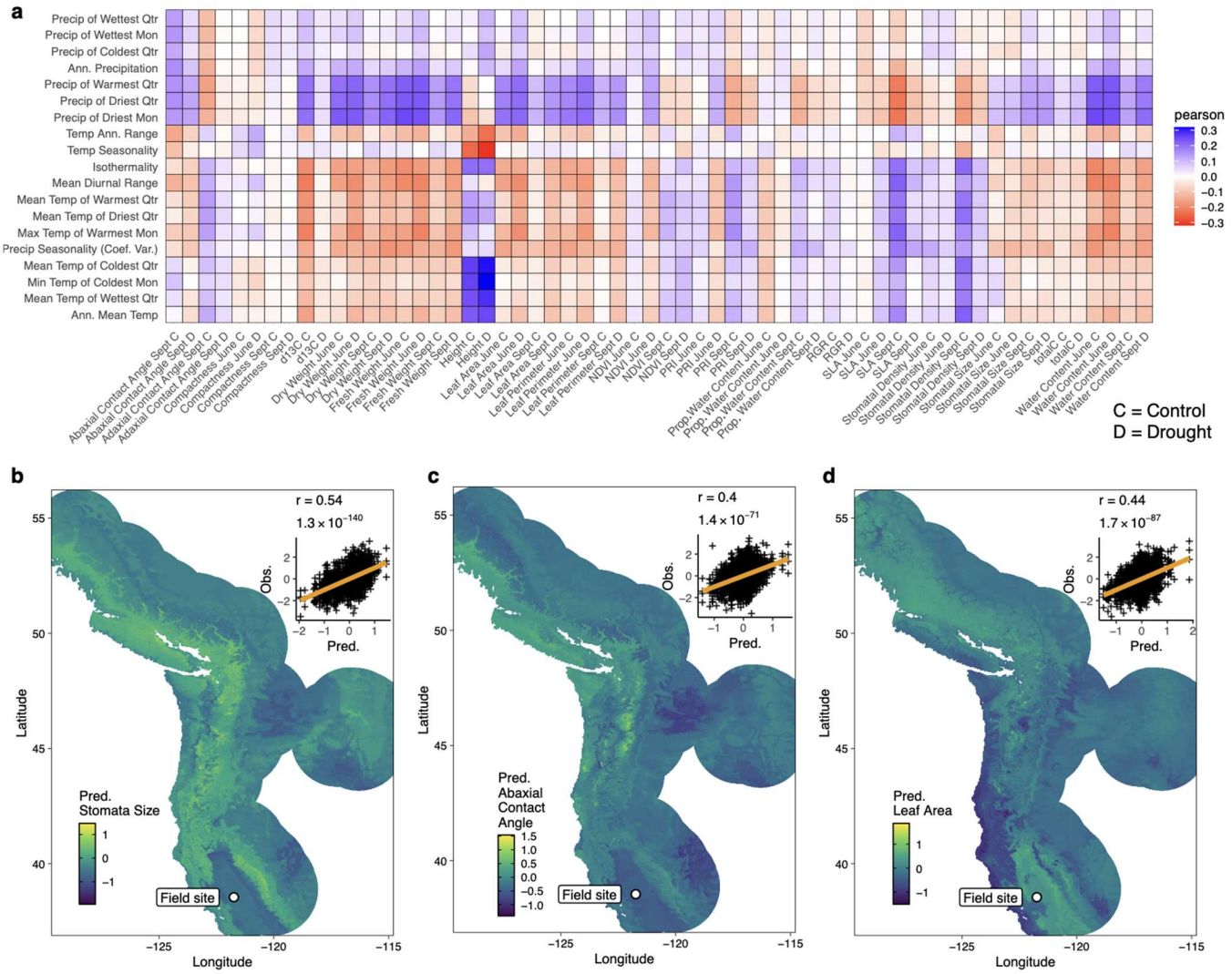

Figure 3. Analyses of traits in relation to climate-of-origin among *P. trichocarpa* genotypes. (a) Heatmap illustrating Pearson correlations between stomatal traits and bioclimatic variables sourced from WorldClim. (**b-d)** Geographic distribution of predicted (**b)** stomatal size, (**c)** abaxial contact angle and (**d)** leaf area based on Random Forest models (trait ~ bio climatic variables), with scatter plot inset contrasting predicted versus observed values.

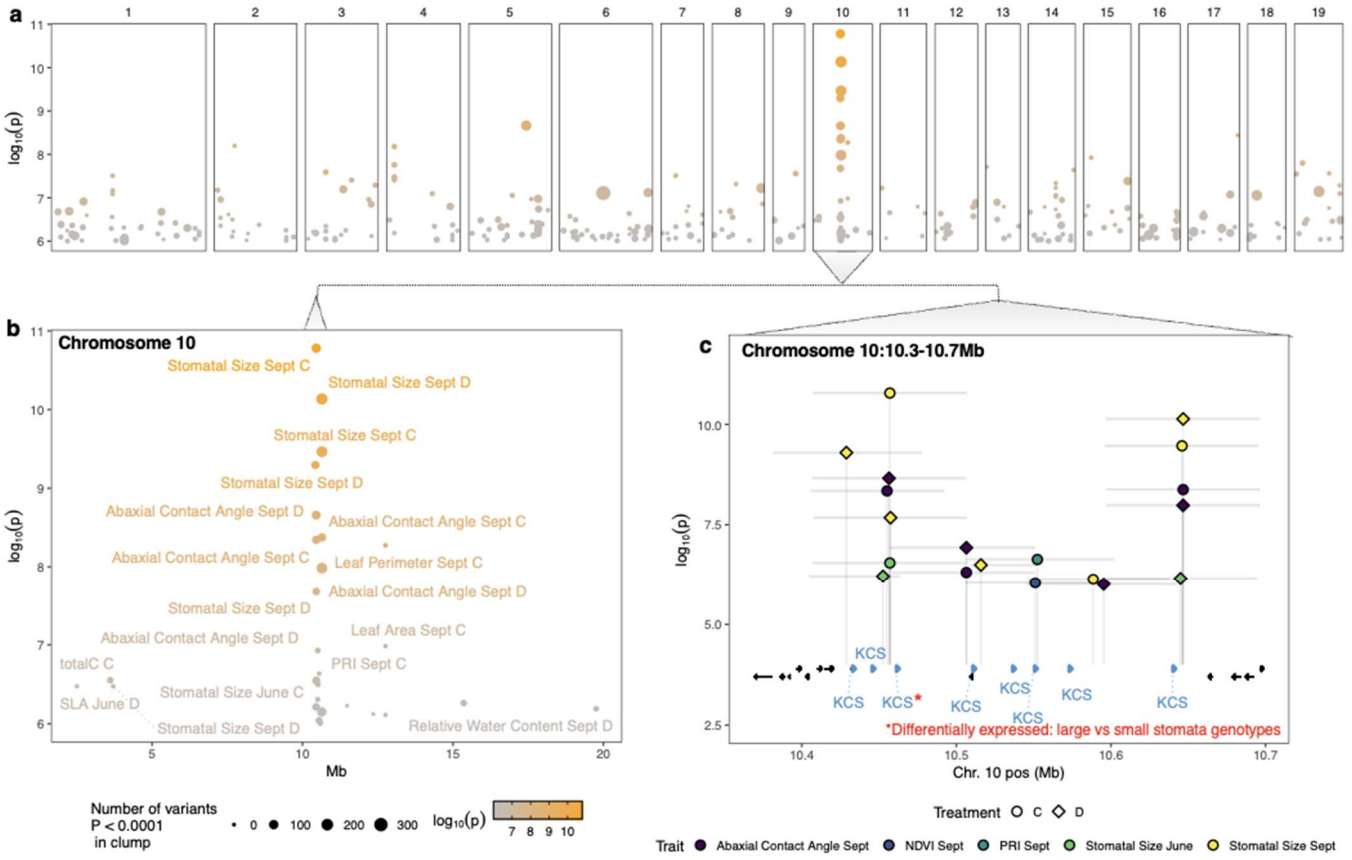

Figure 4. Genome-Wide Association Study (GWAS) reveals locus contributing to stomatal size. **(a)** Summary of GWAS across all traits. Points indicate the positions of clumps identified along the *P. trichocarpa* genome associated with trait variation. The color and size of points reflect the legend in **b**. See Supplemental Figure 6 for GWAS results annotated per trait. **(b)** A zoom-in view of peaks on Chromosome 10. **(c)** High-resolution view of a prominent genomic region on Chromosome 10, focusing on the interval containing significant clumps. Annotated genes within this region are highlighted, with KCS genes highlighted by blue colors. The vertical lines show the positions and significance of clumps for associations with specific traits. Horizontal lines indicate the range of variants within each clump. The KCS gene Potri.010G079500, the only differentially expressed gene between large and small stomata genotypes, found in a GWAS region, is marked with an asterisk, motivating future work to identify specific causal variant.

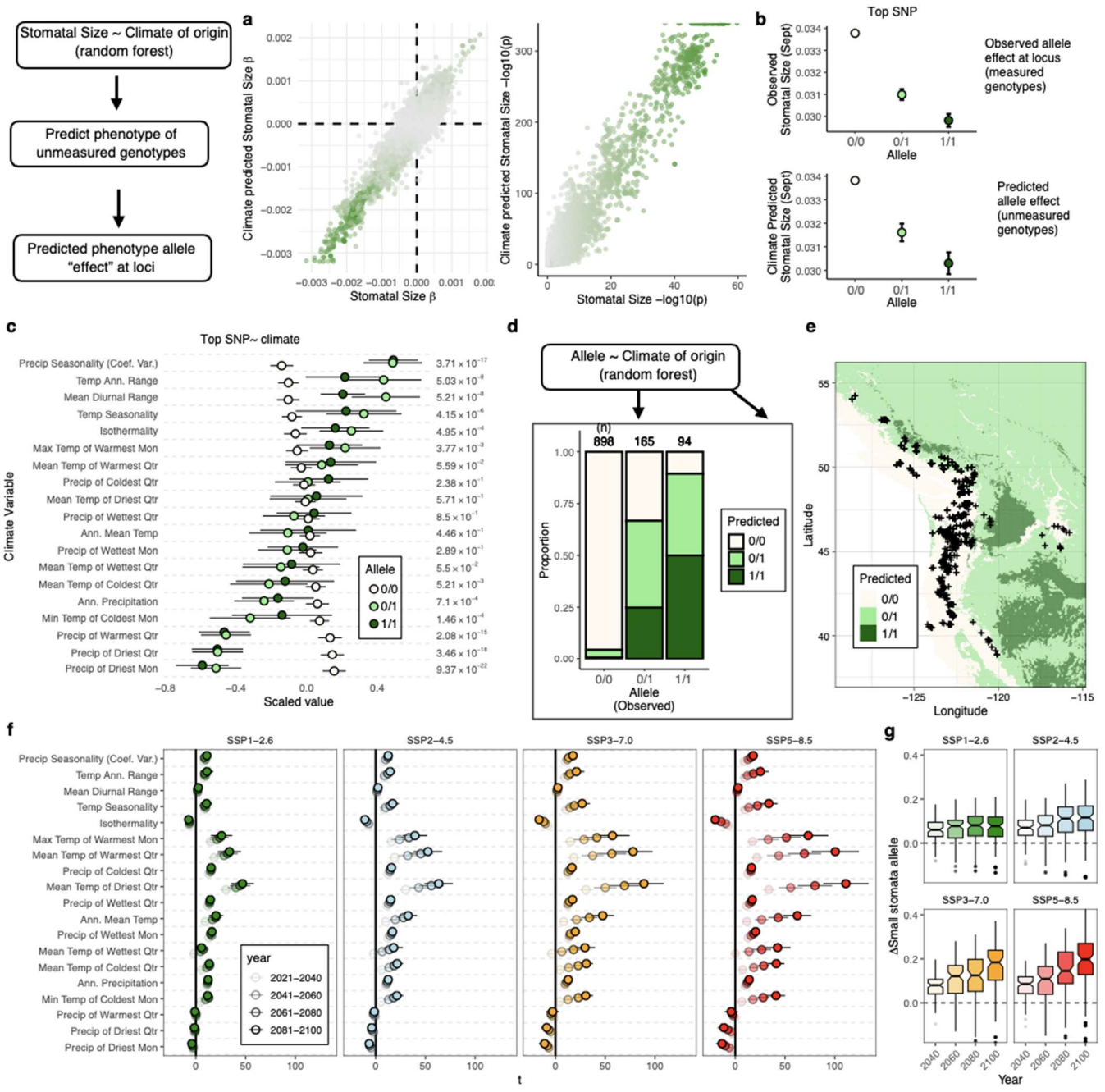

Figure 5. Analysis of Locus on Chromosome 10 (10,356,950 – 10,746,695) associated with Stomatal Size. (a) left: Allele effects on stomatal size (left:β, right: -log10(p) from simple linear regression phenotype~allele across all observations and ”allele effects” on climate-predicted allele effects of genotypes with unmeasured phenotypes in region on Chromosome 10. (**b)** Depiction of allele effect on stomatal size for genotypes with measured (upper) and climate-predicted (lower) phenotypes. Each point illustrates the mean, while error bars represent ± 2 standard errors. **(c)** T-statistic values from Pearson Correlation, illustrating the relationship between allele state and the climate origin of genotypes. **(d)** Visualization of the prediction accuracy of the random forest model, presenting the proportion of predicted allele states corresponding to each observed allele. **(e)** Geographical mapping of predicted allele states based on bioclimatic variables.

(f) Change in bioclimatic variables from historical measures under various climate scenarios (SSPs and time). X-axis (T) represents t-test difference between future and current measures. Points mark mean values, where error bars indicate standard error across 10 GCM models. **(g)** Predicted change in frequency of small stomata allele on Chromosome 10 under future climates. Boxplots represent predictions averaged across GCM models for 100 iterations of randomized, balanced training sets for random forest models of genotype ~ bioclim variables under contemporary climates, used to predict genotype states at *P. trichocarpa*.

Supplemental Materials

Supplemental Materials and Methods

NA.

Supplemental figures

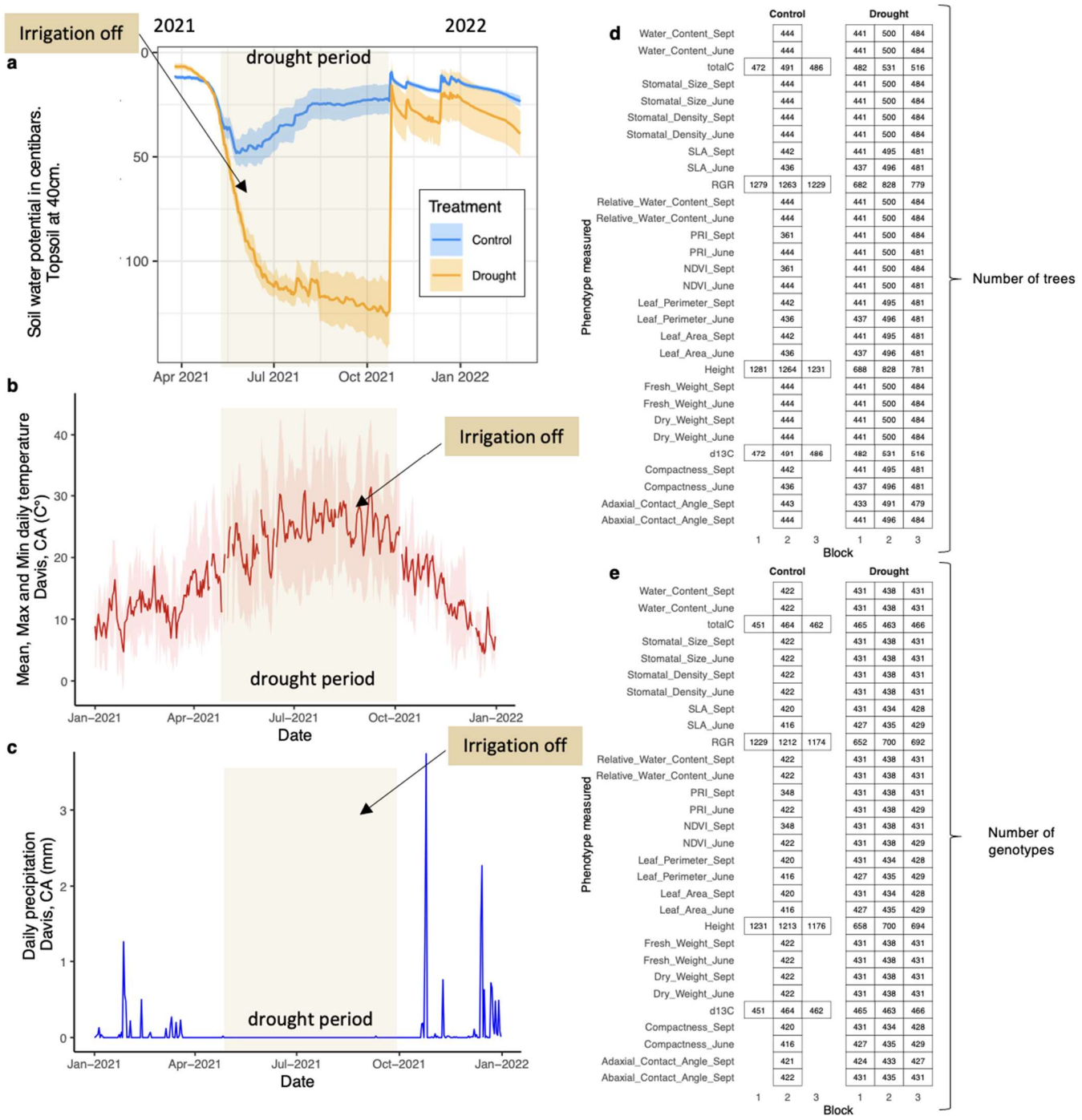

Figure S1. Soil water potential, Davis, CA climate data and experimental design. (a) Soil mean water potential at 40 cm depth. Data derived from gypsum block water marks installed across drought and control treatments (control = blue; drought = orange) field site from March 2021 until February 2022. The ribbon around the graph line represents standard error. In **(b)** the Mean, Max and Min daily temperature and **(c)** Daily precipitation from Davis, California from March 2021 until January 2022 are shown. Data from: "DAVIS 2 WSW EXPERIMENTAL FARM, CA US USC00042294", (38.5349°, -121.7761°), www.ncei.noaa.gov. **(d)** Number of trees and **(e)** Number of genotypes per phenotype measured.

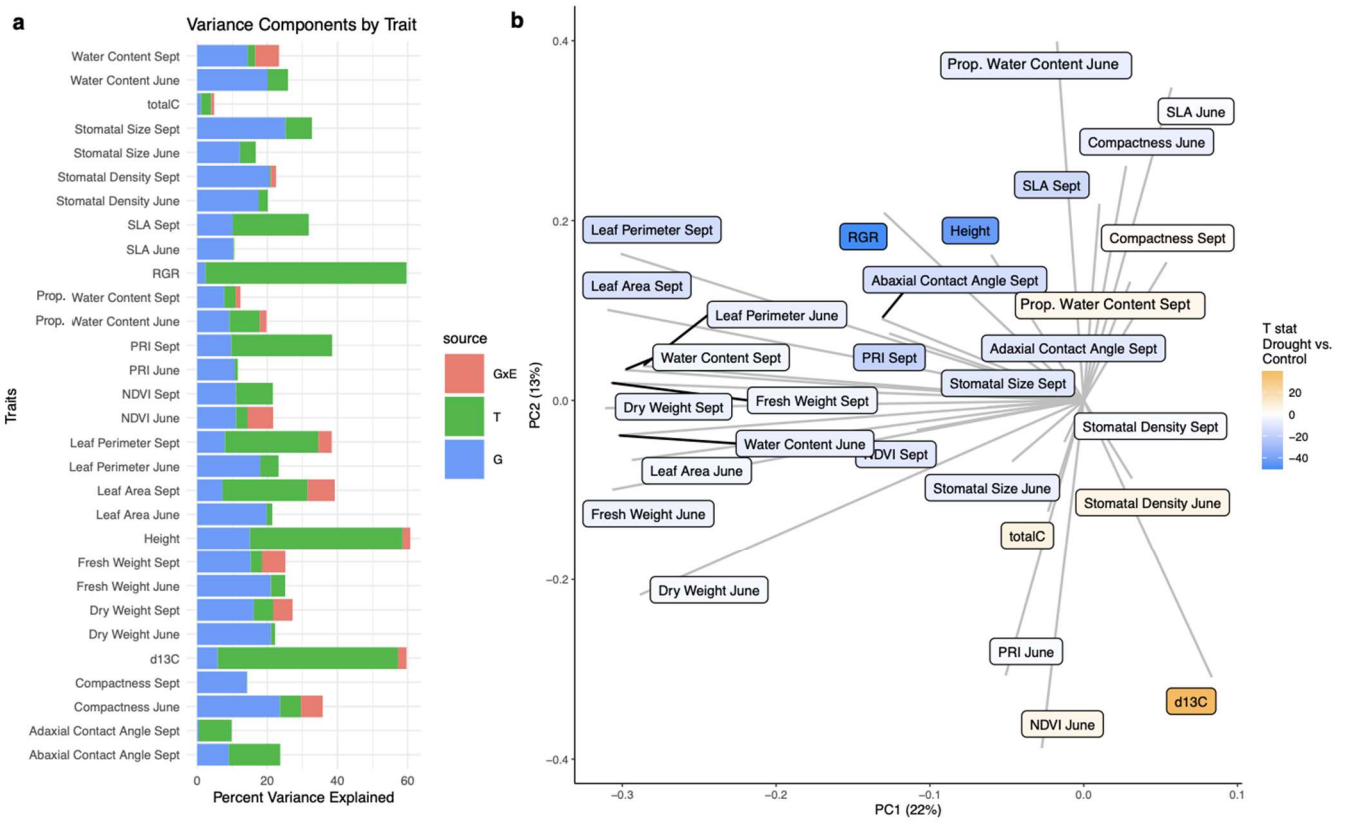

Figure S2. Variance components analysis a and Principal Component Analysis b by trait. (a) The stacked bar chart represents the distribution of variance components for stomatal and leaf plant traits, assessed in two months: June and September. Variance sources are color-coded: genetic (G) in blue, environmental (T) in green, and genotype by environment interaction (GxE) in red. The x-axis displays the percentage variance explained, while the y-axis lists the specific traits under investigation. For several traits, the GxE interaction explains a substantial proportion of the observed variance, emphasizing the importance of considering both genetic and environmental factors in trait expression. **(b)** Principal Component Analysis (PCA) Scatter Plot of 14 Different Leaf Traits visualizing the variation of 14 different leaf traits between the two treatments, control and drought. The horizontal axis, PC1, explains 26% of the variance, while the vertical axis, PC2, accounts for 12% of the variance.

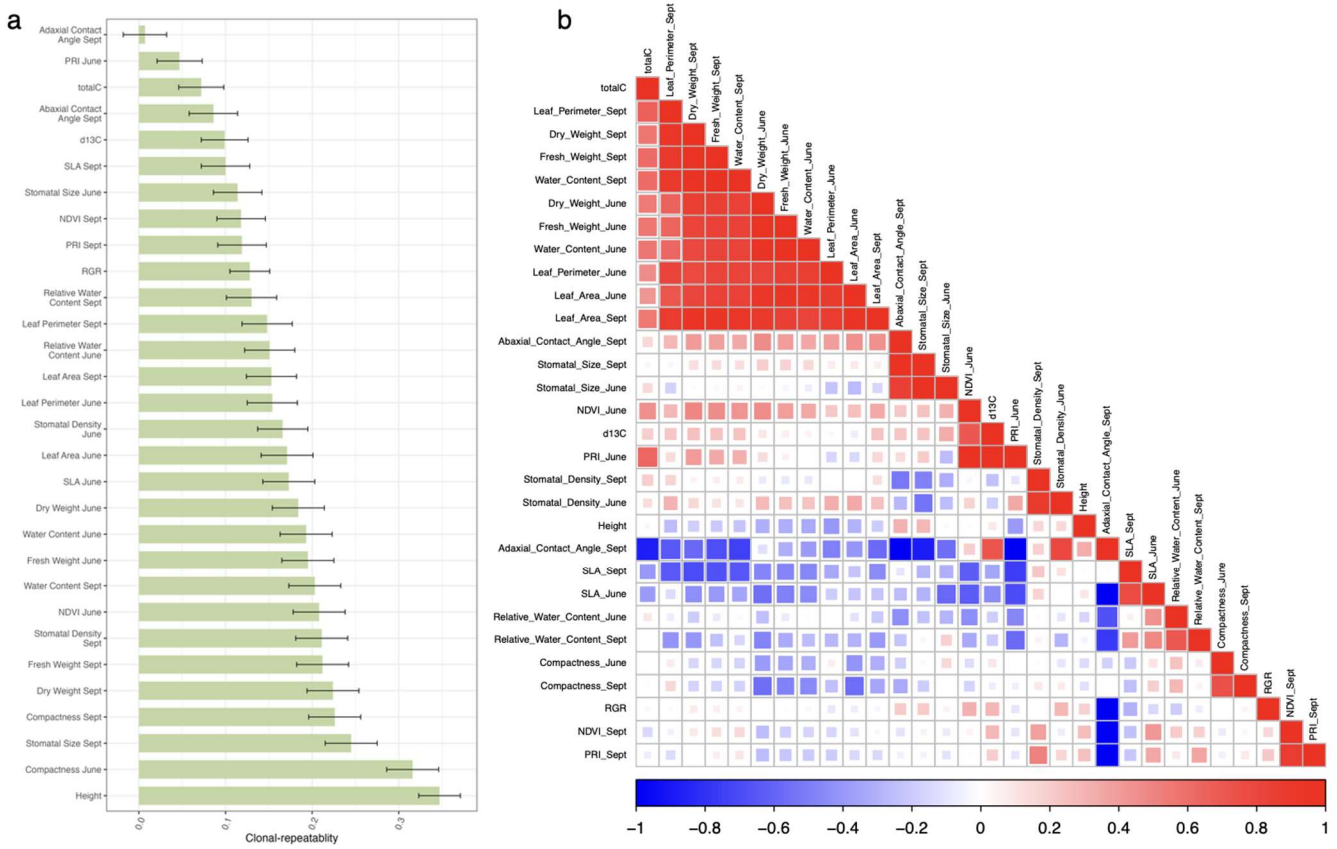

Figure S3: Genetic control of traits in the GWAS population: (a) bar graph represents estimated total genetic variance as a proportion of phenotypic variance (y-axis) for each trait (x-axis). Error bars indicate the standard error of the estimates. **(b)** Genetic correlation of traits in the population: each cell represents the genetic correlation between pairs of traits measured for this population. The color and the intensity of each cell reflects the sign and magnitude of genetic correlation.

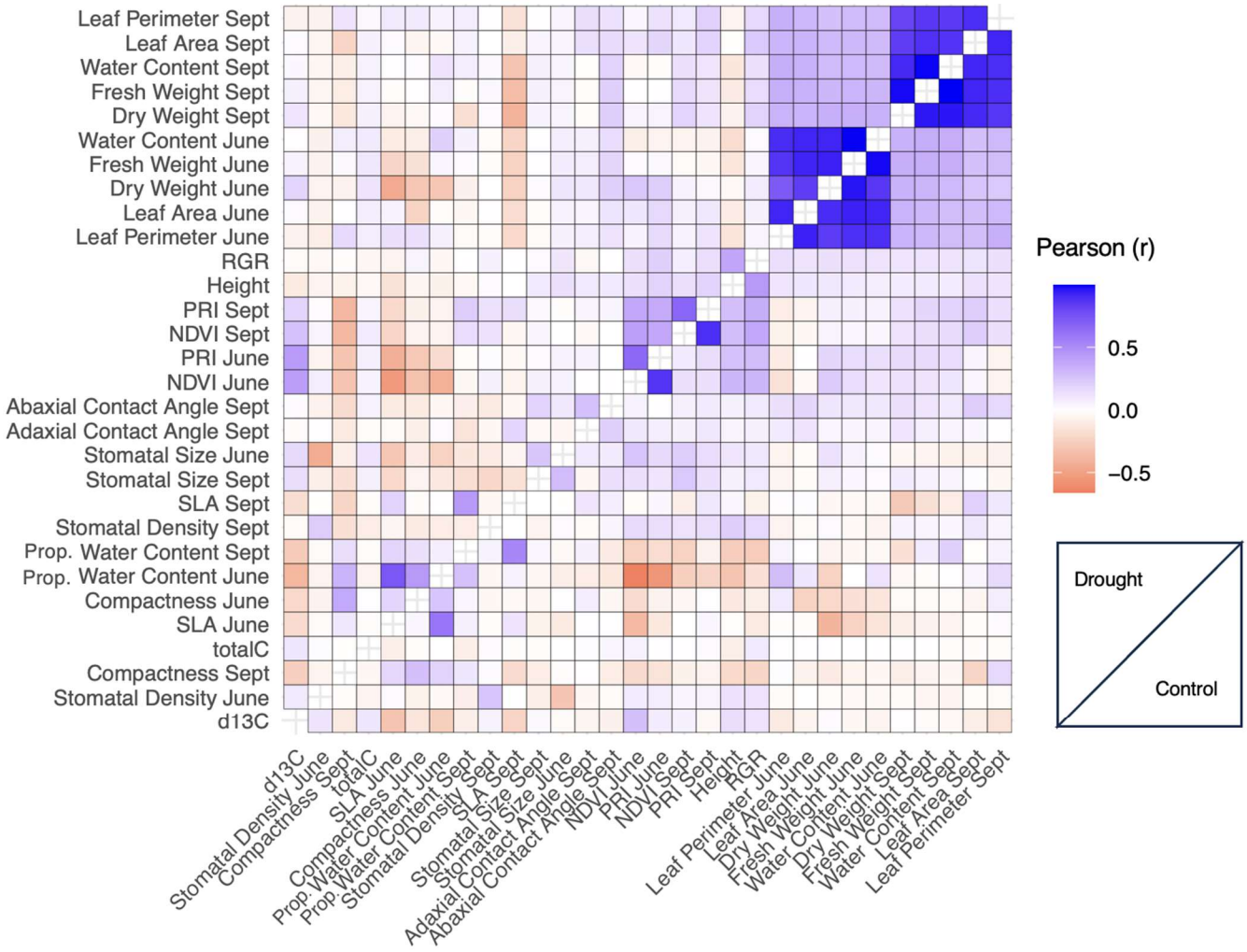

Figure S4. Comparative Analysis (Correlations) of Traits measured in this study. Above the diagonal are traits under drought conditions. Below the diagonal are traits measured under control conditions.

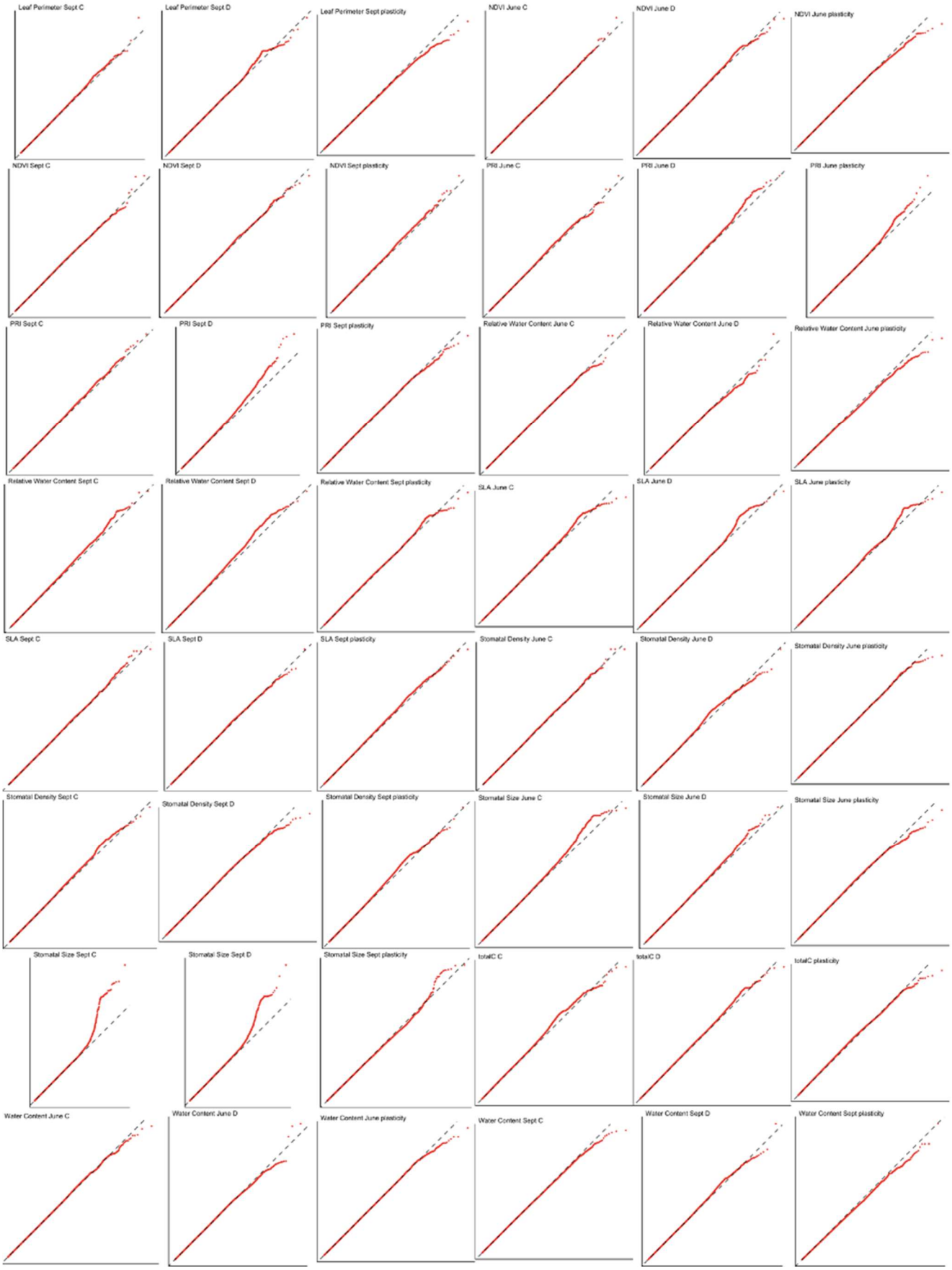
Leaf Perimeter Sept C
Leaf Perimeter Sept D
Leaf Perimeter Sept plasticity
NDVI June C
NDVI June D
NDVI June plasticity
NDVI Sept C
NDVI Sept D
NDVI Sept plasticity
PRI June C
PRI June D
PRI June plasticity
PRI Sept C
PRI Sept D
PRI Sept plasticity
Relative Water Content June C
Relative Water Content June D
Relative Water Content June plasticity
Relative Water Content Sept C
Relative Water Content Sept D
Relative Water Content Sept plasticity
SLA June C
SLA June D
SLA June plasticity
SLA Sept C
SLA Sept D
SLA Sept plasticity
Stomatal Density June C
Stomatal Density June D
Stomatal Density June plasticity
Stomatal Density Sept C
Stomatal Density Sept D
Stomatal Density Sept plasticity
Stomatal Size June C
Stomatal Size June D
Stomatal Size June plasticity
Stomatal Size Sept C
Stomatal Size Sept D
Stomatal Size Sept plasticity
totalC C
totalC D
totalC plasticity
Water Content June C
Water Content June D
Water Content June plasticity
Water Content Sept C
Water Content Sept D
Water Content Sept plasticity

887

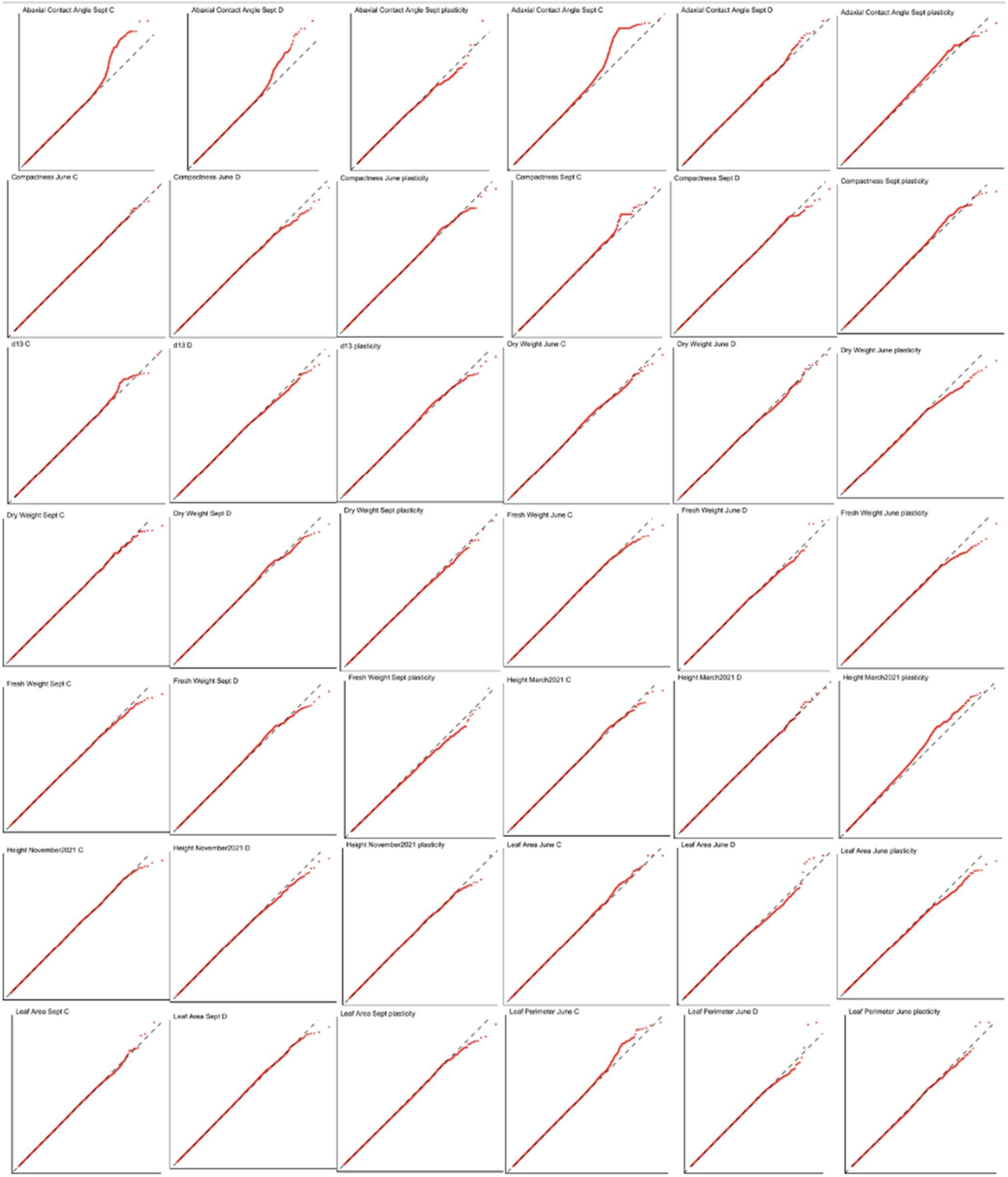

Figure S5. Quantile-quantile (QQ) plots displaying the observed versus expected -log10(p-values) for all traits included in the analysis. The red diagonal line represents y=x, representing the null hypothesis of no association.

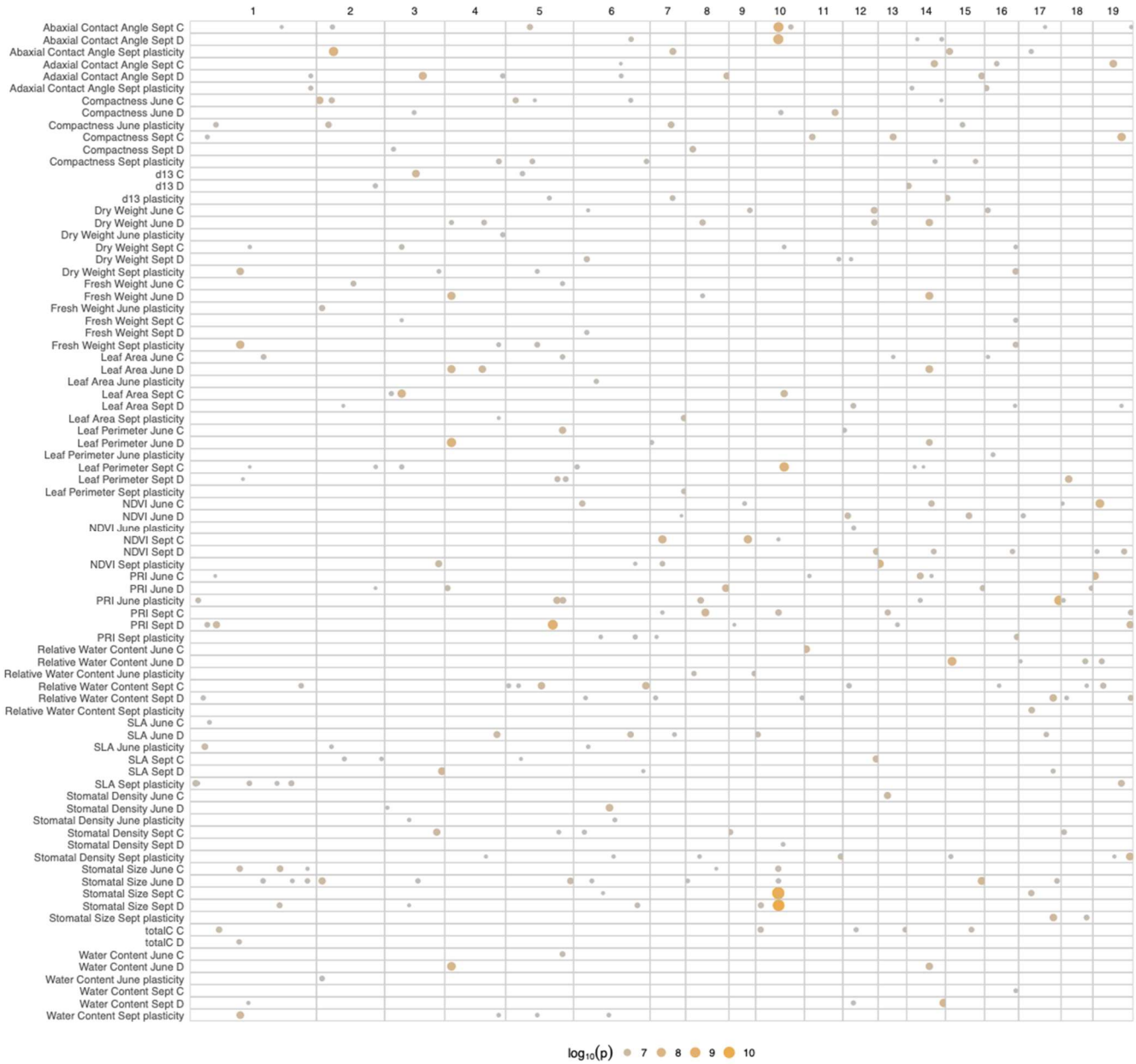

Figure S6: GWAS for all traits. Significant associations (−log 10(p)) are shown across chromosomes. Rows represent traits, columns indicate chromosomes, and dot size reflects association strength, with larger dots indicating higher significance.

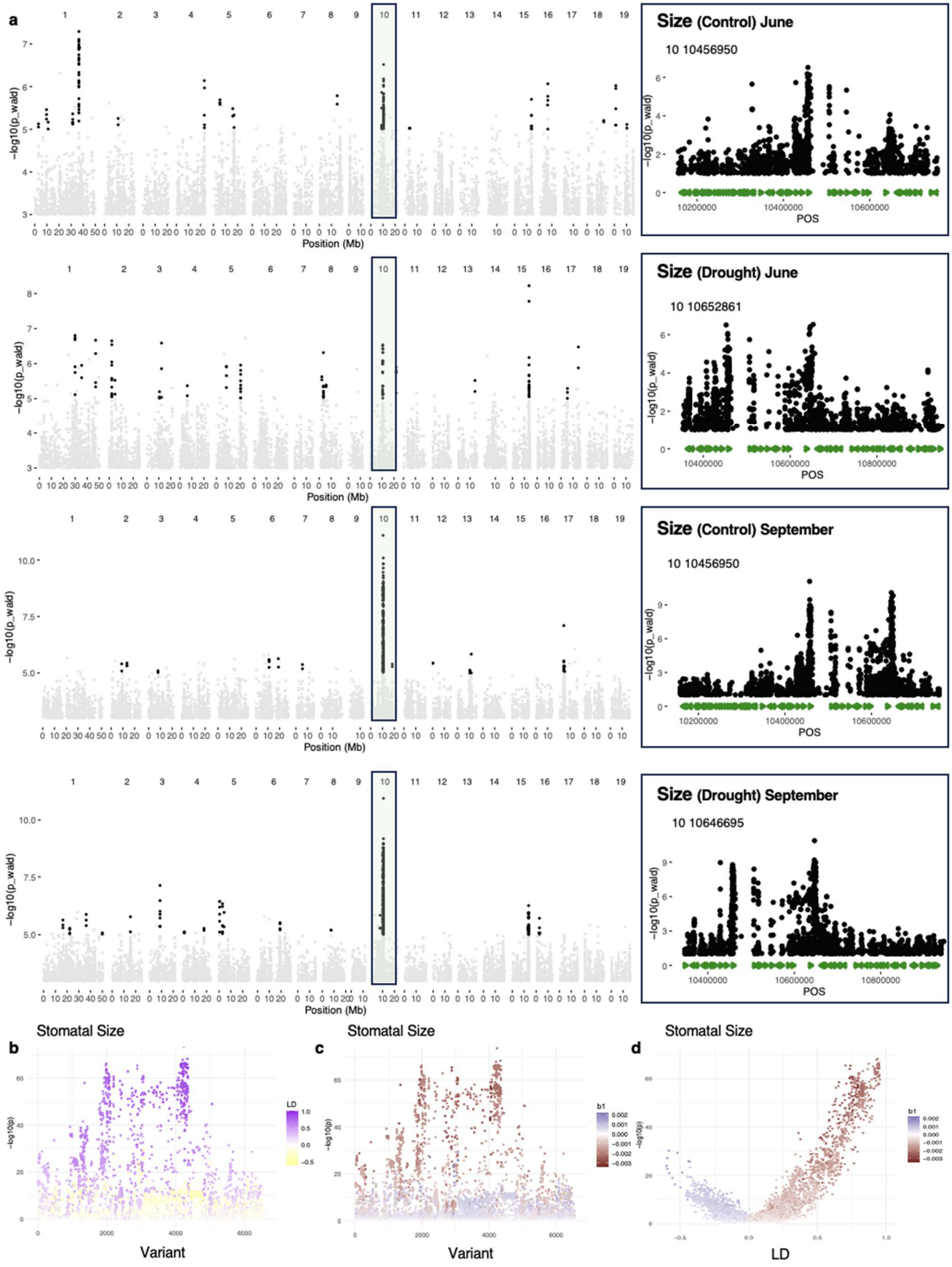
a
Position (Mb)
−log10(p_wald)
Size (Control) June
10 10456950
Size (Drought) June
10 10652861
Size (Control) September
10 10456950
Size (Drought) September
10 10646695
POS
b
Stomatal Size
Variant
c
Stomatal Size
Variant
d
Stomatal Size
LD

Figure S7. Genome-Wide Association Study (GWAS) results for untransformed stomatal size. (a) Stomatal Size in June under control (upper) and drought conditions (lower) and Stomatal Size in September control (upper) and drought conditions (lower). A prominent peak is observed on Chromosome 10 across both environmental conditions and time points. This peak is delineated by the green boxes and further detailed in the zoomed-in panels on the right, which center on the most significant variant. Green icons within the zoomed-in panels mark the positions of *P. trichocarpa* genes. The most significant polymorphisms for each trait are emphasized in the respective panels. (**b-d)**: Effects and linkage disequilibrium locus on Chromosome 10 (10,356,950 – 10,746,695) associated with Stomatal Size. (b) Estimated genetic effect (β and p from simple linear regression phenotype~allele across all observations) on size and density for each variant in this window. **(c)** Estimated LD (Pearson correlation) between all variants and the variant with the most significant association to each trait. **(d)**. Relationship between LD of each variant with the most significant variant and the significance of their association to each trait colored by their estimated genetic effect (β).

910

911

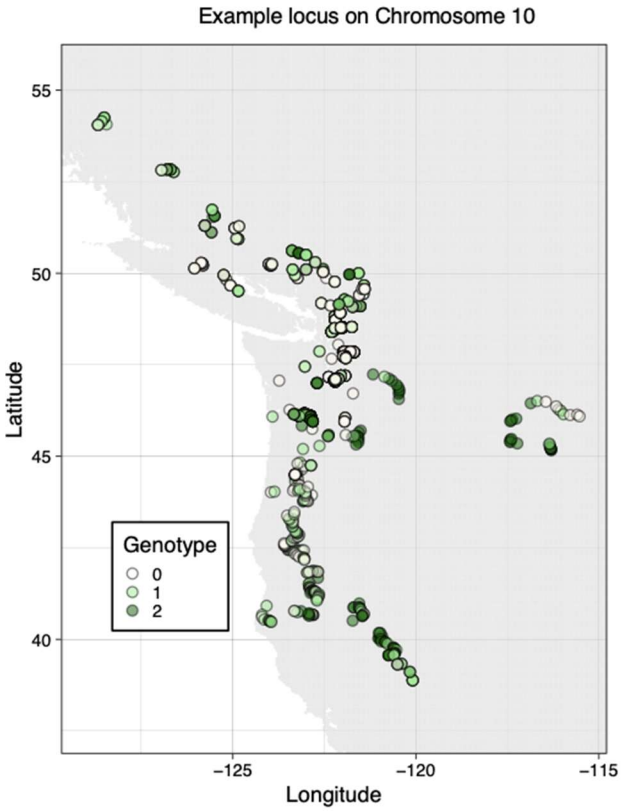

912

913 **Figure S8. Observed geographical distribution of example allele in Chromosome 10 (10,356,950 –**
914 **10,746,695) associated with stomata size and density.**

Supplemental Tables

Supplemental Table 1. Phenotypes measured and used for analysis.

Variable	Tissue	Definition	Unit	Time
Leaf Area	Leaf	Area of the leaf	cm^2	Jun-21
				Sep-21
Leaf Perimeter	Leaf	Perimeter of the leaf	cm	Jun-21
				Sep-21
Compactness	Leaf	$(\text{Perimeter of the leaf})^2$ / Area of the leaf	unitless	Jun-21
				Sep-21
Stomatal Density	Leaf	Stomatal number per mm^2	$/mm^2$	Jun-21
				Sep-21
Stomatal Size	Leaf	Stomatal size (pore length)	mm	Jun-21
				Sep-21
Fresh weight	Leaf	Fresh weight of the leaf	gram	Jun-21
				Sep-21
Dry weight	Leaf	Dry weight of the leaf	gram	Jun-21
				Sep-21
Water Content	Leaf	Fresh weight - Dry weight	gram	Jun-21
				Sep-21
Proportional Water Content	Leaf	(Fresh weight - Dry weight) / Fresh weight	unitless	Jun-21
				Sep-21

Adaxial Contact Angle	Leaf	Contact Angle of adaxial surface	degrees	Sep-21
Abaxial Contact Angle	Leaf	Contact Angle of abaxial surface	degrees	Sep-21
δ13C	Wood	ratio of the two stable isotopes of carbon ^{13}C and ^{12}C	per mil, ‰	Jan-22
NDVI	Leaf	Normalized Difference Vegetation Index Reference: Rouse et al. (1974) Equation: NDVI = (R800-R680)/(R800+R680)	unitless	Jun-21 Sep-21
PRI	Leaf	Photochemical Reflectance Index Reference: Gamon et al. (1992) Equation: PRI = (R531- R570) / (R531+ R570)	unitless	Sep-21 Sep-21

Supplemental Table 2. Raw phenotypes.

Raw_data_stomata_paper2024

Supplemental Table 3. (Min/max/average) for each phenotype measured.

Statistic	Units	Min	Max	Median	Mean	SD
Stomatal_Density_Sept	/mm2	38.8555281	413.88518	173.083716	176.451563	45.890872
Stomatal_Density_June	/mm2	31.152648	409.924488	182.46551	187.539294	55.8886263
Stomatal_Size_Sept	mm	0.01726802	0.04656731	0.03309701	0.03292914	0.00365149
Stomatal_Size_June	mm	0.01594699	0.0425358	0.030936	0.030632	0.00400338

			8	53	88	
Fresh_Weight_June	gram	0.281	5.082	1.277	1.38063404	0.57545124
Dry_Weight_June	gram	0.094	1.675	0.414	0.4483743	0.19379044
Water_Content_June	gram	0.187	3.407	0.857	0.93225974	0.39418538
Fresh_Weight_Sept	gram	0.291	9.389	1.4805	1.62760946	0.81675482
Dry_Weight_Sept	gram	0.08	2.777	0.5025	0.55198066	0.27749549
Water_Content_Sept	gram	0.063	6.612	0.974	1.0756288	0.55388603
Proportional_Water_Content_June	unitless	0.42426418	0.9431337	0.6705582	0.6751014	0.03660582
Proportional_Water_Content_Sept	unitless	0.04684015	0.8727758	0.6619306	0.6599173	0.04239435
Adaxial_Contact_Angle_Sept	degrees	4.719	111.602	55.356	54.3589127	16.5286165
Abaxial_Contact_Angle_Sept	degrees	16.172	124.276	78.9685	76.3265424	20.5311852
NDVI_Sept	unitless	0.14314833	0.84026268	0.7008746	0.6494610	0.13617428
PRI_Sept	unitless	-0.1525656	0.03866728	-0.0027779	-0.0092965	0.03091265
NDVI_June	unitless	0.04147551	0.86932631	0.7686876	0.7459674	0.08684121
PRI_June	unitless	-0.1172695	0.04743566	0.0170237	0.0119811	0.02076093
Leaf_Area_June	cm^2	11.9396413	148.936951	41.033653	43.644240	16.6227386
Leaf_Perimeter_June	cm	17.5444079	62.678148 5	31.837498	32.353670 1	5.94774078
Compactness_June	unitless	17.1135335	44.111509 8	24.542442 4	25.128952 5	3.49328865
Leaf_Area_Sept	cm^2	7.66225915	230.07155 9	36.039495 2	40.578150 5	21.4482736

Leaf_Perimeter_Sept	cm	15.2010196	72.0552696	30.5274179	31.4797009	7.52928566
Compactness_Sept	unitless	15.5389189	78.4437152	25.274039	26.7317901	6.30794824
d13	per mil, ‰	-33.229284	-22.155004	-26.277355	-26.515073	1.64721672
SLA_June	m²/g	51.9908854	420.159954	97.8831194	101.119327	21.6971424
SLA_Sept	m²/g	21.9467305	266.816884	72.6510223	75.9960902	22.3949958
totalC	gram	967.900514	1935.55806	1421.98325	1417.93866	86.8528506

Supplemental Table 4. Drought Recovery Index

DRI_poplar_stomata

Supplemental Table 5. Genotype information (location, climate).

Location and Climate of Origin - Poplar

Supplemental Table 6. GWAS summary

GWAS_peaks_poplar_stoma

Supplemental Table 7. All Potential Candidate genes (Orthologs to *Arabidopsis thaliana*), also highlighted with 4 categories (Water, Stomata, Guard Cells, ABA)

GWAS_candidates_poplar_stoma

Supplemental Table 8. NCBI SRA accession numbers and genotype IDs for RNA-Seq data in Populus trichocarpa

NCBI SRA accession numbers and genotype IDs for RNA-Seq data in Populus trichocarpa

Supplemental Table 9. Differential gene expression (DEG) results

DEG_results_RNA_p.trichocarpa

References

Anders, C., Hoengenaert, L., & Boerjan, W. (2023). Accelerating wood domestication in forest trees through genome editing: Advances and prospects. *Current Opinion in Plant Biology*, *71*, 102329.

Aparecido, L. M. T., Miller, G. R., Cahill, A. T., & Moore, G. W. (2017). Leaf surface traits and water storage retention affect photosynthetic responses to leaf surface wetness among wet tropical forest and semiarid savanna plants. *Tree Physiology*, *37*(10), 1285–1300.

Auer, P., Reiner, A., & Leal, S. (2016). The effect of phenotypic outliers and non-normality on rare-variant association testing. *European Journal of Human Genetics: EJHG*, *24*, 1188–1194.

Bansal, S., Harrington, C. A., Gould, P. J., & St Clair, J. B. (2015). Climate-related genetic variation in drought-resistance of Douglas-fir (Pseudotsuga menziesii). *Global Change Biology*, *21*(2), 947–958.

Beerling, D. J., & Woodward, F. I. (2008). Changes in land plant function over the Phanerozoic: reconstructions based on the fossil record. *Botanical Journal of the Linnean Society. Linnean Society of London*, *124*(2), 137–153.

Benavides, R., Carvalho, B., Bastias, C. C., López-Quiroga, D., Mas, A., Cavers, S., Gray, A., Albet, A., Alía, R., Ambrosio, O., Aravanopoulos, F., Auñón, F., Avanzi, C., Avramidou, E. V., Bagnoli, F., Ballesteros, E., Barbas, E., Bastien, C., Bernier, F., … Valladares, F. (2021). The GenTree Leaf Collection: Inter- and intraspecific leaf variation in seven forest tree species in Europe. *Global Ecology and Biogeography: A Journal of Macroecology*, *30*(3), 590–597.

Blumstein, M., Richardson, A., Weston, D., Zhang, J., Muchero, W., & Hopkins, R. (2020). A New Perspective on Ecological Prediction Reveals Limits to Climate Adaptation in a Temperate Tree Species. *Current Biology: CB*, *30*(8), 1447–1453.e4.

Bogeat-Triboulot, M. B., Buré, C., Gerardin, T., Chuste, P. A., Le Thiec, D., Hummel, I., Durand, M., Wildhagen, H., Douthe, C., Molins, A., Galmés, J., Smith, H. K., Flexas, J., Polle, A., Taylor, G., & Brendel, O. (2019). Additive effects of high growth rate and low transpiration rate drive differences in whole plant transpiration efficiency among black poplar genotypes. *Environmental and*

Experimental Botany, *166*, 103784.

Brosché, M., Vinocur, B., Alatalo, E. R., Lamminmäki, A., Teichmann, T., Ottow, E. A., Djilianov, D., Afif, D., Bogeat-Triboulot, M.-B., Altman, A., Polle, A., Dreyer, E., Rudd, S., Paulin, L., Auvinen, P., & Kangasjärvi, J. (2005). Gene expression and metabolite profiling of Populus euphratica growing in the Negev desert. *Genome Biology*, *6*(12), R101.

Candido-Ribeiro, R., & Aitken, S. N. (2024). Weak local adaptation to drought in seedlings of a widespread conifer. *The New Phytologist*, *241*(6), 2395–2409.

Cavallaro, A., Carbonell-Silletta, L., Burek, A., Goldstein, G., Scholz, F. G., & Bucci, S. J. (2022). Leaf surface traits contributing to wettability, water interception and uptake of above-ground water sources in shrubs of Patagonian arid ecosystems. *Annals of Botany*, *130*(3), 409–418.

Clifton-Brown, J., Harfouche, A., Casler, M. D., Dylan Jones, H., Macalpine, W. J., Murphy-Bokern, D., Smart, L. B., Adler, A., Ashman, C., Awty-Carroll, D., Bastien, C., Bopper, S., Botnari, V., Brancourt-Hulmel, M., Chen, Z., Clark, L. V., Cosentino, S., Dalton, S., Davey, C., … Lewandowski, I. (2019). Breeding progress and preparedness for mass-scale deployment of perennial lignocellulosic biomass crops switchgrass, miscanthus, willow and poplar. *Global Change Biology. Bioenergy*, *11*(1), 118–151.

Cocozza, C., Cherubini, P., Regier, N., Saurer, M., Frey, B., & Tognetti, R. (2010). Early effects of water deficit on two parental clones of Populus nigra grown under different environmental conditions. *Functional Plant Biology: FPB*, *37*(3), 244–254.

Cook, B. I., Mankin, J. S., & Anchukaitis, K. J. (2018). Climate change and drought: From past to future. *Current Climate Change Reports*, *4*(2), 164–179.

Cortés, A. J., Restrepo-Montoya, M., & Bedoya-Canas, L. E. (2020). Modern Strategies to Assess and Breed Forest Tree Adaptation to Changing Climate. *Frontiers in Plant Science*, *11*, 583323.

Covarrubias-Pazaran, G. (2016). Genome-assisted prediction of quantitative traits using the R package sommer. *PloS One*, *11*(6), e0156744.

Dai, A. (2012). Increasing drought under global warming in observations and models. *Nature Climate*

Change, *3*(1), 52–58.

Depardieu, C., Girardin, M. P., Nadeau, S., Lenz, P., Bousquet, J., & Isabel, N. (2020). Adaptive genetic variation to drought in a widely distributed conifer suggests a potential for increasing forest resilience in a drying climate. *The New Phytologist*, *227*(2), 427–439.

Dittberner, H., Korte, A., & Mettler-Altmann, T. (2018). Natural variation in stomata size contributes to the local adaptation of water-use efficiency in Arabidopsis thaliana. *Molecular*. https://onlinelibrary.wiley.com/doi/abs/10.1111/mec.14838

Doheny-Adams, T., Hunt, L., Franks, P. J., Beerling, D. J., & Gray, J. E. (2012). Genetic manipulation of stomatal density influences stomatal size, plant growth and tolerance to restricted water supply across a growth carbon dioxide gradient. *Philosophical Transactions of the Royal Society of London. Series B, Biological Sciences*, *367*(1588), 547–555.

Dunlap, J. M., & Stettler, R. F. (2001). Variation in leaf epidermal and stomatal traits ofPopulus trichocarpafrom two transects across the Washington Cascades. *Canadian Journal of Botany. Journal Canadien de Botanique*, *79*(5), 528–536.

Evans, L. M., Slavov, G. T., Rodgers-Melnick, E., Martin, J., Ranjan, P., Muchero, W., Brunner, A. M., Schackwitz, W., Gunter, L., Chen, J.-G., Tuskan, G. A., & DiFazio, S. P. (2014). Population genomics of Populus trichocarpa identifies signatures of selection and adaptive trait associations. *Nature Genetics*, *46*(10), 1089–1096.

Ferrero-Serrano, Á., & Assmann, S. M. (2019). Phenotypic and genome-wide association with the local environment of Arabidopsis. *Nature Ecology & Evolution*, *3*(2), 274–285.

Fick, S. E., & Hijman, R. J. (2017). *Worldclim 2: New 1-km spatial resolution climate*.

Food and Agriculture Organization of the United Nations, United Nations International Children's Emergency Fund, World Health Organization, World Food Programme, & International Fund for Agriculture Development. (2018). *The State of Food Security and Nutrition in the World 2018: Building climate resilience for food security and nutrition*. Food & Agriculture Org.

Franks, P. J., & Beerling, D. J. (2009). Maximum leaf conductance driven by CO_2 effects on stomatal

size and density over geologic time. *Proceedings of the National Academy of Sciences*, *106*(25), 10343–10347.

Franks, P. J., Drake, P. L., & Beerling, D. J. (2009). Plasticity in maximum stomatal conductance constrained by negative correlation between stomatal size and density: an analysis usingEucalyptus globulus. *Plant, Cell & Environment*, *32*(12), 1737–1748.

Gonzales-Vigil, E., Hefer, C. A., von Loessl, M. E., La Mantia, J., & Mansfield, S. D. (2017). Exploiting Natural Variation to Uncover an Alkene Biosynthetic Enzyme in Poplar. *The Plant Cell*, *29*(8), 2000–2015.

Gornall, J. L., & Guy, R. D. (2007). Geographic variation in ecophysiological traits of black cottonwood (Populus trichocarpa) (1). *Canadian Journal of Botany. Journal Canadien de Botanique*, *85*, 1202+.

Grattapaglia, D., Silva-Junior, O. B., Resende, R. T., Cappa, E. P., Müller, B. S. F., Tan, B., Isik, F., Ratcliffe, B., & El-Kassaby, Y. A. (2018). Quantitative Genetics and Genomics Converge to Accelerate Forest Tree Breeding. *Frontiers in Plant Science*, *9*, 1693.

Gray, J. E., Holroyd, G. H., van der Lee, F. M., Bahrami, A. R., Sijmons, P. C., Woodward, F. I., Schuch, W., & Hetherington, A. M. (2000). The HIC signalling pathway links CO2 perception to stomatal development. *Nature*, *408*(6813), 713–716.

Hetherington, A. M., & Woodward, F. I. (2003). The role of stomata in sensing and driving environmental change. *Nature*, *424*(6951), 901–908.

Hoegh-Guldberg, O., Jacob, D., & Bindi, M. (2018). Impacts of 1.5 C global warming on natural and human systems. *Global Warming of*. https://helda.helsinki.fi/handle/10138/311749

Huang, X., Xiao, X., Zhang, S., Korpelainen, H., & Li, C. (2009). Leaf morphological and physiological responses to drought and shade in two Populus cathayana populations. *Biologia Plantarum*, *53*(3), 588–592.

Kačík, F., Ďurkovič, J., & Kačíková, D. (2012). Chemical Profiles of Wood Components of Poplar Clones for Their Energy Utilization. *Energies*, *5*(12), 5243–5256.

Kardiman, R., & Ræbild, A. (2018). Relationship between stomatal density, size and speed of opening

in Sumatran rainforest species. *Tree Physiology*, *38*(5), 696–705.

Keller, S. R., Soolanayakanahally, R. Y., Guy, R. D., Silim, S. N., Olson, M. S., & Tiffin, P. (2011). Climate-driven local adaptation of ecophysiology and phenology in balsam poplar, Populus balsamifera L. (Salicaceae). *American Journal of Botany*, *98*(1), 99–108.

King, J. S., Ceulemans, R., Albaugh, J. M., Dillen, S. Y., Domec, J.-C., Fichot, R., Fischer, M., Leggett, Z., Sucre, E., Trnka, M., & Zenone, T. (2013). The Challenge of Lignocellulosic Bioenergy in a Water-Limited World. *Bioscience*, *63*(2), 102–117.

Kwon, D. H., Huh, H. K., & Lee, S. J. (2014). Wettability and impact dynamics of water droplets on rice (Oryza sativa L.) leaves. *Experiments in Fluids*, *55*(3), 1691.

Lagergren, J., Pavicic, M., Chhetri, H. B., York, L. M., Hyatt, P. D., Kainer, D., Rutter, E. M., Flores, K., Bailey-Bale, J., Klein, M., Taylor, G., Jacobson, D., & Streich, J. (2023). Few-Shot Learning Enables Population-Scale Analysis of Leaf Traits in Populus trichocarpa. *arXiv E-Prints*, arXiv:2301.10351.

Liu, C., Muir, C. D., Li, Y., Xu, L., Li, M., Zhang, J., de Boer, H. J., Sack, L., Han, X., Yu, G., & He, N. (2021). Scaling between stomatal size and density in forest plants. In *bioRxiv* (p. 2021.04.25.441252). https://doi.org/10.1101/2021.04.25.441252

Liu, Z., Hikosaka, K., Li, F., & Jin, G. (2020). Variations in leaf economics spectrum traits for an evergreen coniferous species: Tree size dominates over environment factors. *Functional Ecology*, *34*(2), 458–467.

Love, M. I., Huber, W., & Anders, S. (2014). Moderated estimation of fold change and dispersion for RNA-seq data with DESeq2. *Genome Biology*, *15*(12), 550.

Lynch, M., & Walsh, B. (1998). *Genetics and analysis of quantitative traits*. Oxford University Press.

Magney, T. S., Vierling, L. A., Eitel, J. U. H., Huggins, D. R., & Garrity, S. R. (2016). Response of high frequency Photochemical Reflectance Index (PRI) measurements to environmental conditions in wheat. *Remote Sensing of Environment*, *173*, 84–97.

Marron, N., Delay, D., Petit, J.-M., Dreyer, E., Kahlem, G., Delmotte, F. M., & Brignolas, F. (2002).

Physiological traits of two Populus x euramericana clones, Luisa Avanzo and Dorskamp, during a water stress and re-watering cycle. *Tree Physiology*, *22*(12), 849–858.

McKown, A. D., Guy, R. D., Klápště, J., Geraldes, A., Friedmann, M., Cronk, Q. C. B., El-Kassaby, Y. A., Mansfield, S. D., & Douglas, C. J. (2014). Geographical and environmental gradients shape phenotypic trait variation and genetic structure in Populus trichocarpa. *The New Phytologist*, *201*(4), 1263–1276.

McKown, A. D., Guy, R. D., Quamme, L., & Klápště, J. (2014). Association genetics, geography and ecophysiology link stomatal patterning in Populus trichocarpa with carbon gain and disease resistance trade-offs. *Molecular*. https://onlinelibrary.wiley.com/doi/abs/10.1111/mec.12969

McKown, A. D., Klápště, J., Guy, R. D., Corea, O. R. A., Fritsche, S., Ehlting, J., El-Kassaby, Y. A., & Mansfield, S. D. (2019). A role for SPEECHLESS in the integration of leaf stomatal patterning with the growth vs disease trade-off in poplar. *The New Phytologist*, *223*(4), 1888–1903.

McKown, A. D., Klápště, J., Guy, R. D., Geraldes, A., Porth, I., Hannemann, J., Friedmann, M., Muchero, W., Tuskan, G. A., Ehlting, J., Cronk, Q. C. B., El-Kassaby, Y. A., Mansfield, S. D., & Douglas, C. J. (2014). Genome-wide association implicates numerous genes underlying ecological trait variation in natural populations of Populus trichocarpa. *The New Phytologist*, *203*(2), 535–553.

Mehmood, M. A., Ibrahim, M., Rashid, U., Nawaz, M., Ali, S., Hussain, A., & Gull, M. (2017). Biomass production for bioenergy using marginal lands. *Sustainable Production and Consumption*, *9*, 3–21.

Moghaddam, A., Raza, A., Vollmann, J., Ardakani, M. R., Wanek, W., Gollner, G., & Friedel, J. K. (2013). Carbon isotope discrimination and water use efficiency relationships of alfalfa genotypes under irrigated and rain-fed organic farming. *European Journal of Agronomy: The Journal of the European Society for Agronomy*, *50*, 82–89.

Monclus, R., Dreyer, E., Villar, M., Delmotte, F. M., Delay, D., Petit, J.-M., Barbaroux, C., Le Thiec, D., Bréchet, C., & Brignolas, F. (2006). Impact of drought on productivity and water use efficiency in 29 genotypes of Populus deltoides x Populus nigra. *The New Phytologist*, *169*(4), 765–777.

Mulero, G., Jiang, D., Bonfil, D. J., & Helman, D. (2023). Use of thermal imaging and the photochemical

reflectance index (PRI) to detect wheat response to elevated CO2 and drought. *Plant, Cell & Environment*, *46*(1), 76–92.

Ohsumi, A., Kanemura, T., Homma, K., Horie, T., & Shiraiwa, T. (2007). Genotypic Variation of Stomatal Conductance in Relation to Stomatal Density and Length in Rice (Oryza sativa L.). *Plant Production Science*, *10*(3), 322–328.

Pearce, D. W., Millard, S., Bray, D. F., & Rood, S. B. (2006). Stomatal characteristics of riparian poplar species in a semi-arid environment. *Tree Physiology*, *26*(2), 211–218.

Porth, I., & El-Kassaby, Y. A. (2015). Using Populus as a lignocellulosic feedstock for bioethanol. *Biotechnology Journal*, *10*(4), 510–524.

Regier, N., Streb, S., Cocozza, C., Schaub, M., Cherubini, P., Zeeman, S. C., & Frey, B. (2009). Drought tolerance of two black poplar (Populus nigra L.) clones: contribution of carbohydrates and oxidative stress defence. *Plant, Cell & Environment*, *32*(12), 1724–1736.

Sannigrahi, P., Ragauskas, A. J., & Tuskan, G. A. (2010). Poplar as a feedstock for biofuels: A review of compositional characteristics. *Biofuels, Bioproducts & Biorefining*, *4*(2), 209–226.

Savolainen, O., Lascoux, M., & Merilä, J. (2013). Ecological genomics of local adaptation. *Nature Reviews. Genetics*, *14*(11), 807–820.

Schmidt, T., Fernando, A. L., Monti, A., & Rettenmaier, N. (2015). Life Cycle Assessment of Bioenergy and Bio-Based Products from Perennial Grasses Cultivated on Marginal Land in the Mediterranean Region. *Bioenergy Research*, *8*(4), 1548–1561.

Shepherd, T., & Wynne Griffiths, D. (2006). The effects of stress on plant cuticular waxes: Tansley review. *The New Phytologist*, *171*(3), 469–499.

Simões, R., Rodrigues, A., Ferreira-Dias, S., Miranda, I., & Pereira, H. (2020). Chemical composition of cuticular waxes and pigments and morphology of leaves of Quercus suber trees of different provenance. *Plants*, *9*. https://doi.org/10.3390/plants9091165

Somerville, C., Youngs, H., Taylor, C., Davis, S. C., & Long, S. P. (2010). Feedstocks for lignocellulosic biofuels. *Science*, *329*(5993), 790–792.

Stapley, J., Reger, J., Feulner, P. G. D., Smadja, C., Galindo, J., Ekblom, R., Bennison, C., Ball, A. D., Beckerman, A. P., & Slate, J. (2010). Adaptation genomics: the next generation. *Trends in Ecology & Evolution*, *25*(12), 705–712.

Street, N. R., Skogström, O., Sjödin, A., Tucker, J., Rodríguez-Acosta, M., Nilsson, P., Jansson, S., & Taylor, G. (2006). The genetics and genomics of the drought response in Populus. *The Plant Journal: For Cell and Molecular Biology*, *48*(3), 321–341.

Sun, Z., Jin, X., Albert, R., & Assmann, S. M. (2014). Multi-level modeling of light-induced stomatal opening offers new insights into its regulation by drought. *PLoS Computational Biology*, *10*(11), e1003930.

Tang, J., Yang, X., Xiao, C., Li, J., Chen, Y., Li, R., Li, S., Lü, S., & Hu, H. (2020). GDSL lipase occluded stomatal pore 1 is required for wax biosynthesis and stomatal cuticular ledge formation. *The New Phytologist*, *228*(6), 1880–1896.

Tardieu, F. (2022). Different avenues for progress apply to drought tolerance, water use efficiency and yield in dry areas. *Current Opinion in Biotechnology*, *73*, 128–134.

Taylor, G., Bailey-Bale, J. H., Klein, M. C., Milner, S., Chen, J.-G., Muchero, W., Freer-Smith, P., Tschaplinski, T. J., & Tuskan, J. (2024). Harnessing the power of poplar tree natural genetic variation for the development of future sustainable biofuels and bioproducts: a droughted marginal-land experiment for multi-disciplinary investigations. In *bioRxiv* (p. 2024.01.11.575272). https://doi.org/10.1101/2024.01.11.575272

Taylor, G., Donnison, I. S., Murphy-Bokern, D., Morgante, M., Bogeat-Triboulot, M.-B., Bhalerao, R., Hertzberg, M., Polle, A., Harfouche, A., Alasia, F., Petoussi, V., Trebbi, D., Schwarz, K., Keurentjes, J. J. B., Centritto, M., Genty, B., Flexas, J., Grill, E., Salvi, S., & Davies, W. J. (2019). Sustainable bioenergy for climate mitigation: developing drought-tolerant trees and grasses. *Annals of Botany*, *124*(4), 513–520.

Tricker, P. J., Calfapietra, C., Kuzminsky, E., Puleggi, R., Ferris, R., Nathoo, M., Pleasants, L. J., Alston, V., De Angelis, P., & Taylor, G. (2004). Long-term acclimation of leaf production,

development, longevity and quality following 3 yr exposure to free-air CO2 enrichment during canopy closure in Populus. *The New Phytologist*, *162*(2), 413–426.

Tschaplinski, T. J., Tuskan, G. A., & Gunderson, C. A. (1994). Water-stress tolerance of black and eastern cottonwood clones and four hybrid progeny. I. Growth, water relations, and gas exchange. *Canadian Journal of Forest Research. Journal Canadien de La Recherche Forestiere*, *24*(2), 364–371.

Tschaplinski, T. J., Tuskan, G. A., Sewell, M. M., Gebre, G. M., Todd, D. E., & Pendley, C. D. (2006). Phenotypic variation and quantitative trait locus identification for osmotic potential in an interspecific hybrid inbred F2 poplar pedigree grown in contrasting environments. *Tree Physiology*, *26*(5), 595–604.

Tuskan, G. A., Difazio, S., Jansson, S., Bohlmann, J., Grigoriev, I., Hellsten, U., Putnam, N., Ralph, S., Rombauts, S., Salamov, A., Schein, J., Sterck, L., Aerts, A., Bhalerao, R. R., Bhalerao, R. P., Blaudez, D., Boerjan, W., Brun, A., Brunner, A., … Rokhsar, D. (2006). The genome of black cottonwood, Populus trichocarpa (Torr. & Gray). *Science*, *313*(5793), 1596–1604.

U.S. Department of Energy. (2022). *Sustainable Aviation Fuel Grand Challenge Roadmap: Flight Plan for Sustainable Aviation Fuel Report*. Energy.gov. https://www.energy.gov/eere/bioenergy/articles/sustainable-aviation-fuel-grand-challenge-roadmap-flight-plan-sustainable

U.S. Department of Energy. (2024). 2023 Billion-Ton Report: An Assessment of U.S. Renewable Carbon Resources. *DOE*. https://www.energy.gov/sites/default/files/2024-03/beto-2023-billion-ton-report_2.pdf

Viger, M., Rodriguez-Acosta, M., Rae, A. M., Morison, J. I. L., & Taylor, G. (2013). Toward improved drought tolerance in bioenergy crops: QTL for carbon isotope composition and stomatal conductance in*Populus*. *Food and Energy Security*, *2*(3), 220–236.

Viger, M., Smith, H. K., Cohen, D., Dewoody, J., Trewin, H., Steenackers, M., Bastien, C., & Taylor, G. (2016). Adaptive mechanisms and genomic plasticity for drought tolerance identified in European

black poplar (Populus nigra L.). *Tree Physiology*, *36*(7), 909–928.

Webber, M. S., Watson, J., Zhu, J., Jang, J. H., Çağlayan, M., Heyne, J. S., Beckham, G. T., & Román-Leshkov, Y. (2024). Lignin deoxygenation for the production of sustainable aviation fuel blendstocks. *Nature Materials*, *23*(12), 1622–1638.

Wong, C. Y. S., Bambach, N. E., Alsina, M. M., McElrone, A. J., Jones, T., Buckley, T. N., Kustas, W. P., & Magney, T. S. (2022). Detecting short-term stress and recovery events in a vineyard using tower-based remote sensing of photochemical reflectance index (PRI). *Irrigation Science*, *40*(4), 683–696.

Wright, I. J., Dong, N., Maire, V., Prentice, I. C., Westoby, M., Díaz, S., Gallagher, R. V., Jacobs, B. F., Kooyman, R., Law, E. A., Leishman, M. R., Niinemets, Ü., Reich, P. B., Sack, L., Villar, R., Wang, H., & Wilf, P. (2017). Global climatic drivers of leaf size. *Science*, *357*(6354), 917–921.

Wright, I. J., Reich, P. B., Westoby, M., Ackerly, D. D., Baruch, Z., Bongers, F., Cavender-Bares, J., Chapin, T., Cornelissen, J. H. C., Diemer, M., Flexas, J., Garnier, E., Groom, P. K., Gulias, J., Hikosaka, K., Lamont, B. B., Lee, T., Lee, W., Lusk, C., … Villar, R. (2004). The worldwide leaf economics spectrum. *Nature*, *428*(6985), 821–827.

Wu, J., Albert, L. P., Lopes, A. P., Restrepo-Coupe, N., Hayek, M., Wiedemann, K. T., Guan, K., Stark, S. C., Christoffersen, B., Prohaska, N., Tavares, J. V., Marostica, S., Kobayashi, H., Ferreira, M. L., Campos, K. S., da Silva, R., Brando, P. M., Dye, D. G., Huxman, T. E., … Saleska, S. R. (2016). Leaf development and demography explain photosynthetic seasonality in Amazon evergreen forests. *Science*, *351*(6276), 972–976.

Xu, B., Liu, D., Xu, G., Zhang, X., & Bi, L. (2013). A measurement method for contact angle based on Hough Transformation. *Measurement*, *46*(3), 1109–1114.

Zhang, J., Yang, Y., Zheng, K., Xie, M., Feng, K., Jawdy, S. S., Gunter, L. E., Ranjan, P., Singan, V. R., Engle, N., Lindquist, E., Barry, K., Schmutz, J., Zhao, N., Tschaplinski, T. J., LeBoldus, J., Tuskan, G. A., Chen, J.-G., & Muchero, W. (2018). Genome-wide association studies and expression-based quantitative trait loci analyses reveal roles of HCT2 in caffeoylquinic acid biosynthesis and

its regulation by defense-responsive transcription factors in Populus. *The New Phytologist*, *220*(2), 502–516.

Zhang, M., Suren, H., & Holliday, J. A. (2019). Phenotypic and Genomic Local Adaptation across Latitude and Altitude in Populus trichocarpa. *Genome Biology and Evolution*, *11*(8), 2256–2272.

Zhou, X., Jacobs, T. B., Xue, L.-J., Harding, S. A., & Tsai, C.-J. (2015). Exploiting SNPs for biallelic CRISPR mutations in the outcrossing woody perennial Populus reveals 4-coumarate:CoA ligase specificity and redundancy. *The New Phytologist*, *208*(2), 298–301.

Zhou, X., & Stephens, M. (2012). Genome-wide efficient mixed-model analysis for association studies. *Nature Genetics*, *44*(7), 821–824.

U.S. Department of Energy, U.S. Department of Transport, U.S. Department of Agriculture, and U.S. Environmental Protection Agency. (2022). *SAF Grand Challenge Roadmap: Flight Plan for Sustainbale Aviation Fuel*. https://www.energy.gov/eere/bioenergy/articles/sustainable-aviation-fuel-grand-challenge-roadmap-flight-plan-sustainable